

## Giant transposons promote strain heterogeneity in a major fungal pathogen

Emile Gluck-Thaler<sup>1,2,3\*</sup>, Adrian Forsythe<sup>4</sup>, Charles Puerner<sup>5</sup>, Jason E. Stajich<sup>6</sup>, Daniel Croll<sup>1</sup>, Robert A. Cramer<sup>5</sup>, Aaron A. Vogan<sup>4</sup>

<sup>1</sup> Laboratory of Evolutionary Genetics, Institute of Biology, University of Neuchâtel, Neuchâtel, Neuchâtel 2000, Switzerland

<sup>2</sup> Department of Plant Pathology, University of Wisconsin-Madison, Madison, WI 53706, USA

<sup>3</sup> Wisconsin Institute for Discovery, Madison, WI 53706, USA

<sup>4</sup> Systematic Biology, Department of Organismal Biology, Uppsala University, Uppsala, 752 36, Sweden

<sup>5</sup> Department of Microbiology and Immunology, Geisel School of Medicine, Dartmouth College, Hanover, NH 03755 USA

<sup>6</sup> Department of Microbiology and Plant Pathology, University of California-Riverside, Riverside, CA 92521, USA

\* Corresponding author: Tel: +1 608 264 3239; Email: [gluckthaler@wisc.edu](mailto:gluckthaler@wisc.edu)

### ORCIDiDs

Emile Gluck-Thaler: <https://orcid.org/0000-0003-0438-7495>

Adrian Forsythe: <https://orcid.org/0000-0003-1966-9946>

Charles Puerner: <https://orcid.org/0000-0002-4402-0295>

Jason E. Stajich: <https://orcid.org/0000-0002-7591-0020>

Daniel Croll: <https://orcid.org/0000-0002-2072-380X>

Robert A. Cramer: <https://orcid.org/0000-0001-5503-5006>

Aaron A. Vogan <https://orcid.org/0000-0003-2013-7445>

### Key words:

transposable element, transposon, Aspergillosis, *Aspergillus fumigatus*, strain heterogeneity, secondary metabolism

## 1 Abstract

2 Fungal infections are difficult to prevent and treat in large part due to heterogeneity in clinically  
3 relevant phenotypes. However, the genetic mechanisms driving pathogen variation remain poorly  
4 understood. Here, we determined the extent to which *Starships*—giant transposons capable of  
5 mobilizing numerous fungal genes—generate genetic and phenotypic variability in the human  
6 pathogen *Aspergillus fumigatus*. We analyzed 519 diverse strains, including 12 newly sequenced  
7 with long-read technology, to reveal 20 distinct *Starships* that generate genomic heterogeneity  
8 over timescales impacting experimental reproducibility. *Starship*-mobilized genes encode diverse  
9 functions, including biofilm-related virulence factors and biosynthetic gene clusters, and many are  
10 differentially expressed during infection and antifungal exposure in a strain-specific manner.  
11 These findings support a new model of fungal pathogenesis wherein *Starships* mediate variation  
12 in virulence-related gene content and expression. Together, our results demonstrate that  
13 *Starships* are a foundational mechanism generating disease-relevant genotypic and, in turn,  
14 phenotypic heterogeneity in a major human fungal pathogen.

15  
16  
17

## 18 Introduction

19

20 Infectious diseases caused by fungi pose a grave threat to human health. The World Health  
21 Organization recently coordinated a global effort to prioritize research among fungal pathogens  
22 based on unmet research needs and public health importance<sup>1</sup>. Among the pathogens deemed  
23 most important for research include *Aspergillus fumigatus*, a globally ubiquitous human pathogen  
24 causing disease in an estimated 2 million people yearly<sup>2</sup>. Several infectious diseases are caused  
25 by *A. fumigatus*, including invasive pulmonary aspergillosis, which manifests primarily in  
26 immunocompromised individuals with mortality rates of upwards of 85%. The treatment of *A.*  
27 *fumigatus* infections are complicated by the remarkable variation strains display in virulence,  
28 resistance to antifungals, and other infection-relevant traits<sup>3-7</sup>. Strain heterogeneity confounds  
29 “one size fits all” therapies and poses a significant challenge for developing efficacious disease  
30 management strategies<sup>8</sup>. Recent evaluations of the *A. fumigatus* pangenome have revealed  
31 extensive genetic variability underlying variation in clinically-relevant traits such as antifungal  
32 resistance and virulence, yet in many cases, the origins of such variation remain unexplained<sup>9-11</sup>.  
33 Determining the genetic drivers of strain heterogeneity will help accelerate the development of  
34 strain-specific diagnostics and targeted therapies.

35

36 Mobile genetic elements (MGEs) are ubiquitous among microbial genomes and their activities  
37 profoundly shape phenotypic variation<sup>12</sup>. MGE transposition generates structural variation that  
38 directly impacts gene regulation and function<sup>13-15</sup>, and many elements also modulate genome  
39 content by acquiring genes as “cargo” and transposing them within and between genomes,  
40 facilitating gene gain and loss<sup>16,17</sup>. The ability to generate contiguous genome assemblies with  
41 long-read sequencing technologies has dramatically enhanced our ability to find new lineages of  
42 MGEs<sup>12,18</sup>. For example, *Starships* are a recently discovered superfamily of MGEs found across  
43 hundreds of filamentous fungal taxa<sup>19-21</sup>. *Starships* are fundamentally different from other fungal  
44 MGEs because they are typically 1-2 orders of magnitude larger (~20-700 kb versus 1-8kb) and  
45 carry dozens of protein-coding genes encoding fungal phenotypes. In addition to flanking short  
46 direct repeats, all *Starships* possess a “captain” tyrosine recombinase at their 5’ end that is both  
47 necessary and sufficient for transposition<sup>20</sup>. Many *Starships* make key contributions to adaptive  
48 phenotypes: For example, *Horizon* and *Sanctuary* carry the ToxA virulence factor that facilitates  
49 the infection of wheat, and *Hephaestus* and *Mithridate* encode resistance against heavy metals  
50 and formaldehyde, respectively<sup>22-25</sup>. *Starships* are further capable of horizontal transfer,  
51 implicating them in the acquisition, dissemination and repeated evolution of diverse traits ranging  
52 from host interactions to stress resistance<sup>19,20,23-25</sup>. However, we know little about how *Starships*  
53 drive genetic and phenotypic variation in species relevant for human disease.

54

55 Here, we conduct the first systematic assessment of *Starship* activity and expression in a human  
56 fungal pathogen to test the hypothesis that these unusual MGEs are a source of clinically-relevant  
57 strain heterogeneity. We reveal that *Starships* are responsible for generating previously  
58 unexplainable variation in genome content and structure, including among different isolates of

59 what are purported to be the same laboratory strain. Our interrogation of 507 diverse clinical and  
60 environmental strains of *A. fumigatus*, combined with highly contiguous assemblies of 12 newly  
61 sequenced strains, enabled an unprecedented quantification of *Starship* diversity. We leveraged  
62 the wealth of functional data available for *A. fumigatus* to draw causal links between *Starship*-  
63 mediated genetic variation and phenotypic heterogeneity in secondary metabolite and biofilm  
64 production contributing to pathogen survival and virulence. We analyzed multiple transcriptomic  
65 studies and determined that variation in *Starship* cargo expression arises from strain- and  
66 treatment-specific effects. By revealing *Starships* as a mechanism generating clinically-relevant  
67 phenotypic variation, our work sheds light on the origins of strain heterogeneity and establishes  
68 a predictive framework to decipher the intertwining impacts of transposons on fungal  
69 pathogenesis and human health.

## 70 Results

### 71 Data curation and long-read sequencing

72  
73 *Starships* are difficult to detect in short-read assemblies due to their large size and frequent  
74 localization in regions with high repetitive content<sup>19</sup>. The wealth of publicly available short-read  
75 genomes are still of high value, however, due to the breadth of sampling they provide. We  
76 therefore deployed a hybrid sampling strategy that enabled an accurate and precise accounting  
77 of how *Starships* impact strain heterogeneity. We downloaded 507 short-read *A. fumigatus*  
78 assemblies isolated from environmental and clinical sources that span the known genetic diversity  
79 of this species and used Oxford Nanopore to sequence 12 additional strains with long-read  
80 technology, for a combined total of 519 assemblies<sup>9,10</sup>. The 12 isolates selected for long-read  
81 sequencing were chosen because they represent commonly utilized laboratory strains, clinical  
82 isolates and environmental strains from three major *A. fumigatus* clades<sup>9</sup>. We performed short-  
83 read Illumina sequencing of the 12 strains to provide additional support and error-correct the long-  
84 read assemblies. The long-read assemblies are of reference quality, representing nearly full  
85 chromosome assemblies with an L50 range of 4-5 and a N50 range of 1.9-4.7 Mb, and are thus  
86 ideal for investigating the connection between *Starships* and strain heterogeneity (Table S1).

### 87 At least 20 distinct *Starships* vary among *A. fumigatus* strains

88  
89 We began evaluating the impact of *Starships* on strain heterogeneity by systematically annotating  
90 them in the 519 assemblies using the starfish workflow<sup>21</sup>. We identified a total of 787 individual  
91 *Starships* and validated these predictions by manually annotating a subset of 86 elements (Table  
92 S2, Table S3, Methods)<sup>9,10</sup>. As expected, more *Starships* were recovered in total from short-read  
93 assemblies, but on average more *Starships* were recovered from each reference-quality  
94 assembly, highlighting the utility of our hybrid sampling approach (Fig. S1).  
95

96 To determine how many different *Starships* generate variability in *A. fumigatus*, we assigned each  
97 *Starship* element to a family (based on similarity to a reference library of captain tyrosine  
98 recombinases), a *navis* (Latin for “ship”; based on orthology of the *A. fumigatus* captains) and a  
99 *haplotype* (based on k-mer similarity scores of the cargo sequences; Methods), following Gluck-  
100 Thaler and Vogan 2024. For example, *Starship Osiris h4* belongs to *haplotype* 4 within the *Osiris*  
101 *navis*, which is part of the Enterprise-family. Using a conservative threshold that required  
102 observing the same *navis-haplotype* (i.e., *Starship*) at multiple sites, we identified 20 high-  
103 confidence *Starships* that met these criteria and 34 medium-confidence *Starships* that did not,  
104 revealing a phylogenetically and compositionally diverse set of *Starships* actively transposing  
105 within *A. fumigatus* (Methods, Table 1, Fig. 1, Table S4, Table S5).

106

107 *Starships* distributions are heterogeneous and only partially explained by  
108 strain relatedness

109

110 All high-confidence *Starships* show polymorphic presence/absence variation, representing a  
111 previously unexamined source of genetic heterogeneity across *A. fumigatus* strains (Fig. 1A,  
112 Table S6). For example, the two commonly used reference strains Af293 and CEA10 carry 12  
113 different high-confidence *Starships*, but share only 4 in common (or only 2, using a more  
114 conservative threshold of not counting fragments or degraded elements; Fig. 1D, Table S7). The  
115 number of high-confidence *Starships* per long-read isolate ranges from 0-11 (median = 3, std.  
116 dev. = 3.5)<sup>26,27</sup>. To identify the underlying drivers of variation in *Starship* distributions, we  
117 investigated the relationship between *Starship* repertoires and strain relatedness by testing if  
118 phylogenetic signal underlies *Starship* distributions. We genotyped *Starship* presence/absence in  
119 the best sampled clade of *A. fumigatus* with well resolved phylogenetic relationships and good  
120 representation of environmental and clinical strains (Clade 1 *sensu* Lofgren et al., 2022, n = 150)  
121 and found that isolate relatedness is significantly but only weakly correlated with similarity in  
122 *Starship* repertoire (Fig. 1E, Table S8, Spearman's  $\rho = 0.29$ ;  $P < 2.2e^{-16}$ , using the genotyping  
123 dataset). This indicates that *Starships* are a source of genetic heterogeneity among even closely  
124 related strains. While we are unable to unequivocally differentiate horizontal transfer events from  
125 sexual or parasexual recombination in *A. fumigatus*, we hypothesize that horizontal transfer within  
126 this species is at least partially responsible for generating the observed patchy distributions of  
127 *Starships*, since *Starship* transfer has occurred between fungal species of vastly different  
128 taxonomic ranks, and barriers to transfer would be lower within species.

129 *Starships* actively transpose in clones of reference laboratory strains

130

131 We determined the short-term potential for *Starships* to introduce unwanted variation into  
132 laboratory experiments by comparing lab-specific isolates of the same strain used by different  
133 research groups. First, we found that *Starship* insertions in the reference Af293 genome coincide

Family	Name	Predicted target site	Mean length in bp (SD)	Type element	Functions of interest in type element
Tardis	<i>Tardis h1</i>	TACGGAGTAG	81,743 (9,347)	W72310-lr_s00161	GH71, SAH
Prometheus	<i>Gnosis h1</i>	A(N <sub>3</sub> )CTA(N <sub>17</sub> )T	82,313 (23,570)	A-fum-AFUG-100413-0667_s00261	GH18, lysM
Prometheus	<i>Gnosis h2</i>	-	93,292 (60)	CM2733_s04518	bafY, fumihopaside A BGC
Phoenix	<i>Janus h1</i>	-	62,365 (19,076)	F14513G_s04800	CHROMO
Phoenix	<i>Janus h2</i>	A(N <sub>3</sub> )TTACTA(N <sub>2</sub> )A(N <sub>15</sub> )CT	217,821 (102,982)	47-4_s00005	CHROMO, DHDPS, GH18, GH71
Phoenix	<i>Janus h3</i>	A(N <sub>3</sub> )TTACTA(N <sub>2</sub> )A(N <sub>15</sub> )CT	42,070 (37,412)	SF1S6_s05434	CHROMO
Phoenix	<i>Janus h4</i>	-	19,097 (5,047)	CM6458_s04616	CHROMO
Phoenix	<i>Janus h5</i>	-	34,546 (18,524)	47-10_s00011	CHROMO
Enterprise	<i>Osiris h1</i>	5S rDNA	37,633 (2,148)	A-fum-AFIS-13708-CDC-14_s00209	putative BGC
Enterprise	<i>Osiris h2</i>	5S rDNA	138,260 (2,424)	B5269_s04148	ARS, B-LAC, COP
Enterprise	<i>Osiris h3</i>	5S rDNA	70,476 (28,148)	Afu-218-E11_s00395	bafB, hrmB
Enterprise	<i>Osiris h4</i>	5S rDNA	51,342 (13,227)	Af293_s00032	putative BGC
Galactica	<i>Lamia h1</i>	A(N)TAGT	69,899 (24,972)	S02-30_s00148	GH18, lysM
Galactica	<i>Lamia h2</i>	A(N)TAGT	65,414 (6,136)	ATCC42202_s00060	fumigermin BGC
Galactica	<i>Lamia h3</i>	A(N)TAGT	236,680 (74,695)	ISSF-21_s05253	GH18, GH71
Galactica	<i>Lamia h4</i>	A(N)TAGT	291,189 (215,918)	F7763_s04695	bafX, fumigermin BGC, GH3, GH18, GH71, GT8, GT31
Prometheus	<i>Logos h1</i>	A(N <sub>10</sub> )TACTTATTA(N)A(N <sub>6</sub> )A	69,008 (5,313)	CEA10-lr_s00105	bafZ
Prometheus	<i>Logos h2</i>	-	56,189 (31,755)	CEA10-lr_s00103	bafC
Hephaestus	<i>Neb h1</i>	TTACA(N <sub>5</sub> )AAT	48,346 (5,585)	AF293_s00037	ARS, bafA, cgnA, hrmA
Hephaestus	<i>Neb h2</i>	TTACA(N <sub>5</sub> )AAT	54,751 (7,226)	AF293_s00031	ARS

Table 1: High Confidence *Starships* in *Aspergillus fumigatus*. Abbreviations: GH: glycosyl hydrolase; GT: glycosyl transferase; SAH: salicylate hydroxylase; DHDPS: dihydrodipicolinate synthetase; CHROMO: chromatin modification domain; ARS: arsenic resistance cluster; COP: copper resistance; B-LAC: Beta-lactamase

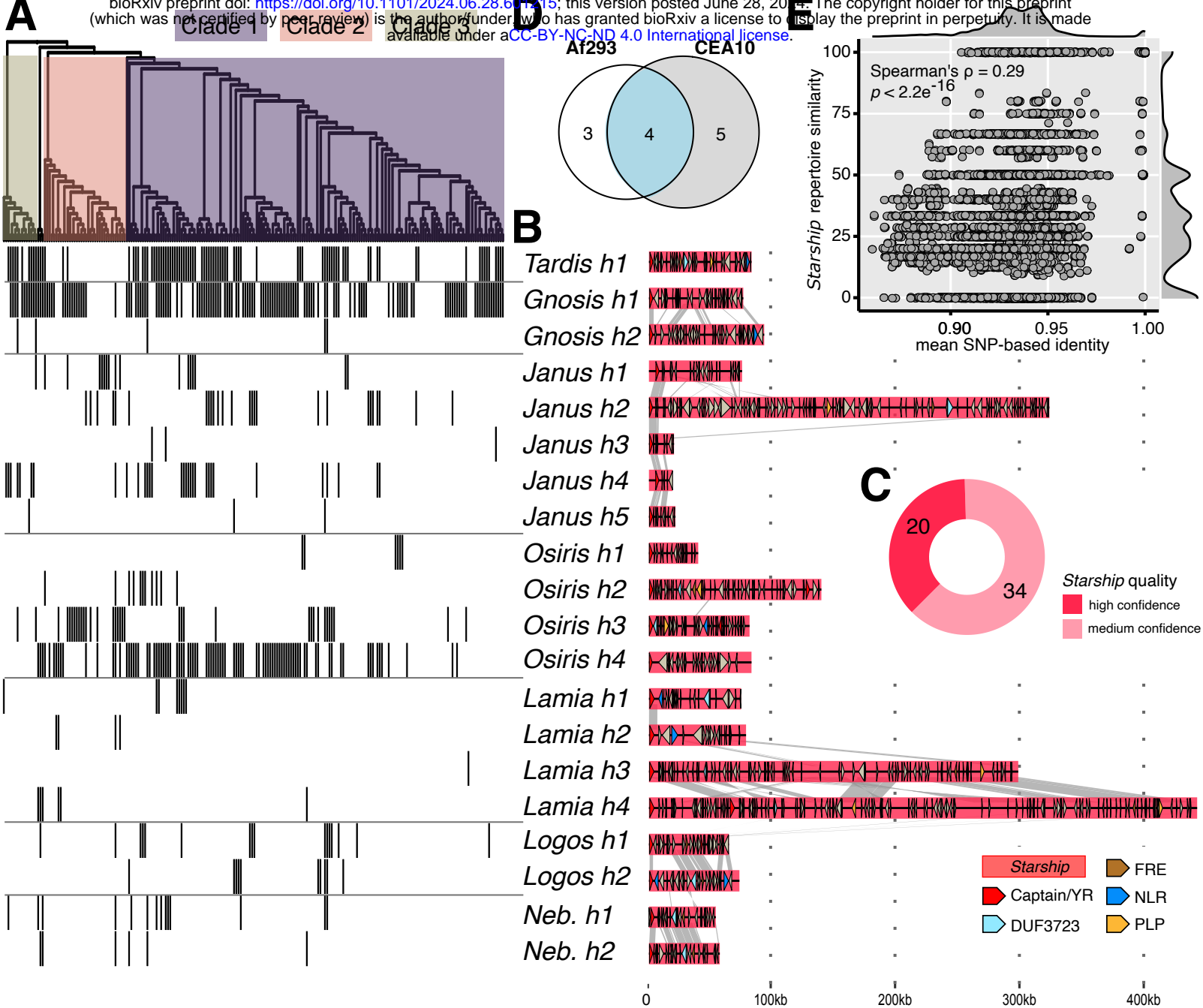


Figure 1: At least 20 distinct Starships carrying hundreds of protein-coding genes vary in their presence/absence across *Aspergillus fumigatus* strains. A) Top: a SNP-based maximum likelihood tree of 220 *A. fumigatus* strains, color-coded according to phylogenetic clade (sensu Lofgren et al., 2022)9. Bottom: A heatmap depicting the presence (gray) and absence (white) of 20 high-confidence Starships in each isolate. B) Schematics and sequence alignments of the type elements from 20 high-confidence Starships, where links between schematics represent alignable regions  $\geq 500$ bp and  $\geq 80\%$  nucleotide sequence identity and arrows represent predicted coding sequences. C) A donut chart summarizing the number of distinct types of Starships by the quality of their prediction. D) A Venn diagram indicating the number of shared and unique high-confidence Starships in the reference strains Af293 and CEA10 (Table S7). E) A scatterplot depicting pairwise comparisons of SNP-based Identity by State (IBS) and Jaccard similarity in high-confidence Starship presence/absence profiles between 150 Clade 1 strains (Table S8).

134 with 4/8 known putative structural variants identified in other Af293 strains (Table S9), suggesting  
135 that *Starship* transposition and/or loss contributes substantially to structural variation observed  
136 among isolates of what should otherwise be clones of the same strain<sup>5</sup>. We complemented this  
137 literature-based approach with a genomics approach where we compared sequence data among  
138 isolates of the same strain. We compared the locations of *Starships* between the CEA10  
139 assembly we generated here and a publically available CEA10 assembly (BioSample  
140 SAMN28487501), and found evidence that at least 1 *Starship* (*Nebuchadnezzar h1*) has jumped  
141 to a different chromosomal location, from chromosome 6 to chromosome 4 (Fig. S2). We also  
142 evaluated *Starship* heterogeneity in three additional strains with both publicly available short-read  
143 data and long-read data generated in this study. One of the strains (ATCC-46645-Ir) showed signs  
144 of *Starship* heterogeneity among isolates used by different research groups. Specifically, a small  
145 number of reads (a single mapped read for *h2* and three for *h1*) supported precise excision events  
146 for *Nebuchadnezzar h1* and *h2*, suggesting these elements have transposed or have been lost in  
147 a subset of the nuclei within one of the sequenced isolates (Fig. S3). This suggests that *Starships*  
148 are active under laboratory conditions, which is directly relevant for experimental design in this  
149 case as *Nebuchadnezzar h1* carries the HAC gene cluster known to impact biofilm-associated  
150 virulence (see below)<sup>28</sup>. Additionally, one breakpoint of a large-scale reciprocal translocation  
151 between chromosomes 1 and 6 among CEA10 isolates is localized precisely within a *Starship*,  
152 suggesting that this structural variant was caused by the presence of the *Starship*, an association  
153 that has also been noted in at least one other species<sup>19</sup>. Together, *Starship*-mediated variation  
154 among isolates of the same *A. fumigatus* strain suggests these transposons cause genomic  
155 instability over short-enough timescales that they may affect routine laboratory work and  
156 experimental reproducibility.

## 157 *Starships* mobilize upwards of 16% of accessory genes that differ across 158 strains

159  
160 *A. fumigatus* strains differ extensively in the combinations of genes found in their genomes,  
161 resulting in a large and diverse pangenome<sup>9,10</sup>. To quantify how much pangenomic variation is  
162 attributable to actively transposing *Starships*, we estimated the total proportion of genomic content  
163 present in the 20 high-confidence *Starships* (Fig. 2, Methods). We examined these *Starships* in  
164 the 13 reference-quality assemblies (Af293 plus the 12 newly sequenced long-read strains) and  
165 found that between 0-2.4% of genomic nucleotide sequence (and 0-2.1% of all genes per  
166 genome) is mobilized as *Starship* cargo (Fig. 2A). We then built a pangenome with all 519 strains  
167 and extracted all orthogroups (i.e., genes) found in the 13 reference-quality genomes to gain  
168 insight into the distribution of *Starship*-associated gene content (Table S10). Across the 13 isolate  
169 pangenome, 2.9% of all genes, which corresponds to 9.7% of all accessory and singleton genes,  
170 have at least 1 member carried as *Starship* cargo (Fig. 2B). Accessory and singleton genes are  
171 overrepresented in *Starships*, with ~92% of *Starship* genes being either accessory or singleton  
172 compared with 24.6% of non-*Starship* associated genes. We determined the upper bounds of this  
173 conservative estimate by examining the 13 isolate pangenome in the context of all 54 high- and

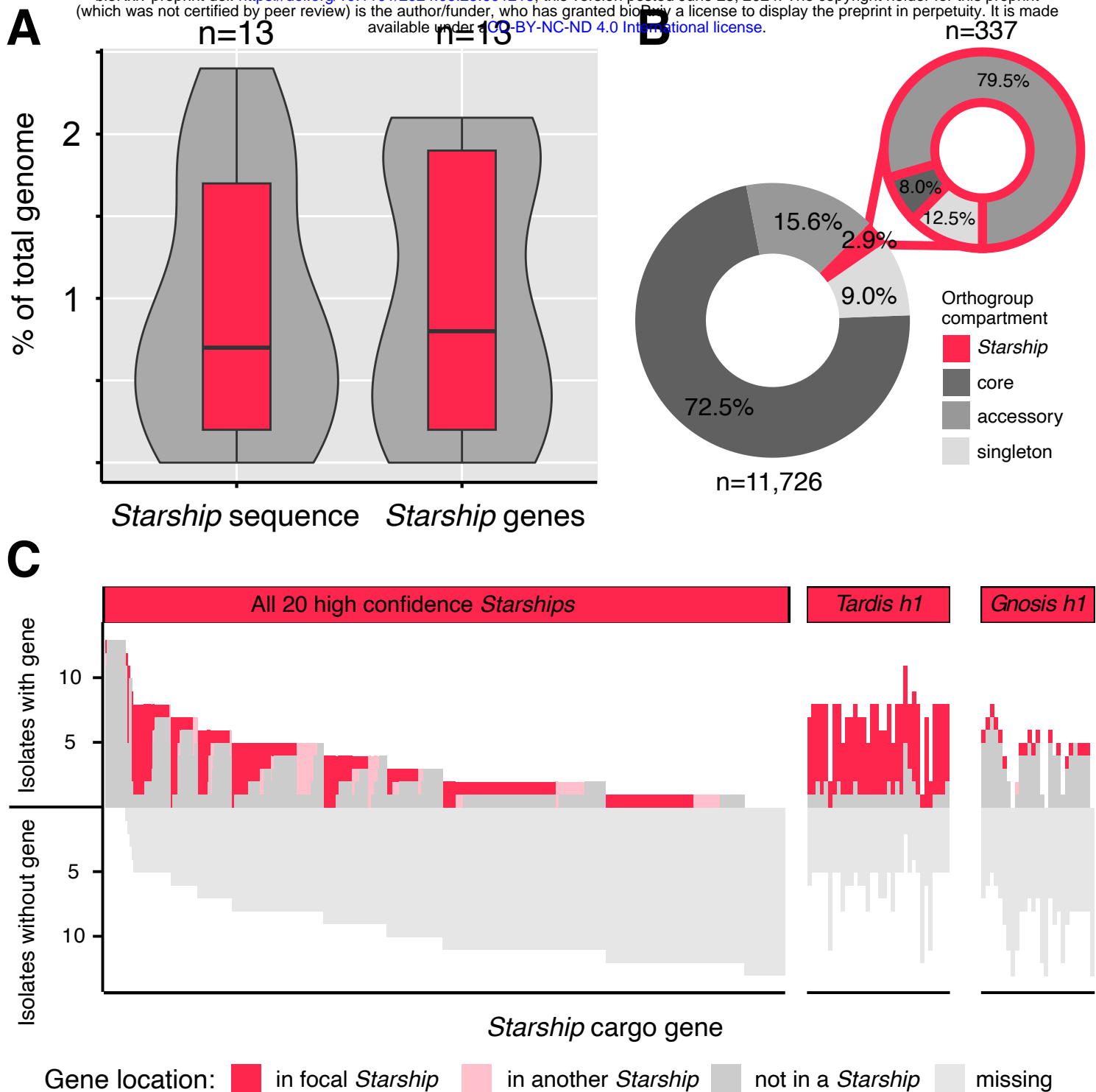


Figure 2: Starships are enriched in accessory genes whose presence/absence and genomic location vary across *Aspergillus fumigatus* strains. All panels visualize data derived from 13 reference-quality *A. fumigatus* assemblies and the 20 high-confidence Starships ( $n = 459$  elements total). A) Box-and-whisker plots summarizing the total percentage of nucleotide sequence and predicted genes carried by Starships per genome. B) Donut charts summarizing the percentages of gene orthogroups in the core, accessory, singleton, and Starship-associated compartments of the *A. fumigatus* pangenome (Table S10). C) Iceberg plots summarizing the genomic locations of the single best BLASTp hits ( $\geq 90\%$  identity,  $\geq 33\%$  query coverage) to the cargo genes from the type elements of all 20 high-confidence Starships (left) and two individual Starships (right; Table S12). Each column in the iceberg plot represents a cargo gene and is color-coded according to the genomic location of hits (full dataset in Fig. S4).

174 medium-confidence *Starships*, and found that 4.8% of all genes, representing 16% of all  
175 accessory and singleton genes, have at least 1 member carried as *Starship* cargo (Fig. S4, Table  
176 S11). Together, these data reveal a previously hidden association between *Starships* and the  
177 making of *A. fumigatus*' accessory pangenome.

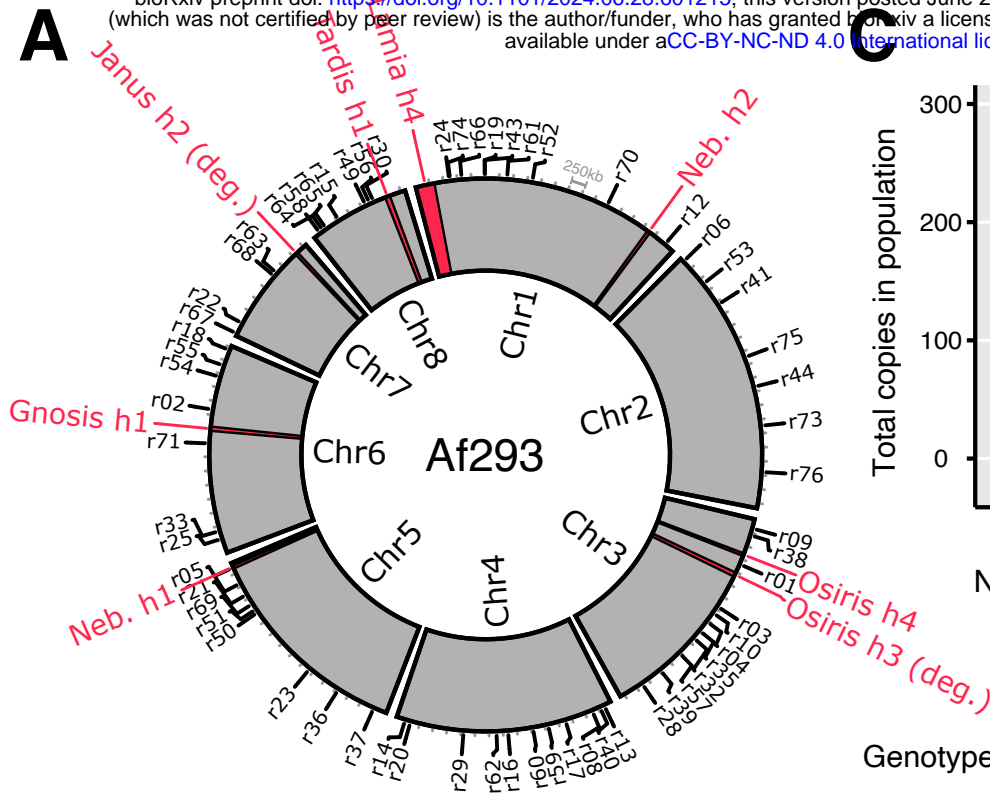
## 178 *Starships* differ in their potential to mediate gain and loss of unique sequence

179  
180 We further determined the potential for *Starships* to introduce variation into *A. fumigatus* strains  
181 by testing if *Starship* genes are uniquely found in those elements or found elsewhere in the  
182 genome. We calculated the degree of association between a given cargo gene and a *Starship* by  
183 identifying the genomic locations of best reciprocal BLAST hits to genes in the 20 high-confidence  
184 type elements (Fig. 2C, Fig. S5, Table S12, Table S13, Methods). Across the 13 reference-quality  
185 assemblies, we found that the vast majority of *Starship* genes display presence/absence variation  
186 between strains (i.e., are accessory or singleton) although several genes are present in conserved  
187 regions in these particular strains (while seemingly counter-intuitive, these genes do vary in their  
188 presence/absence and are *Starship*-associated when examining the larger 519 strain population,  
189 as expected). We found that many genes are almost always carried as cargo in active *Starships*  
190 when present in a given genome (e.g., the majority of cargo on *Tardis h1*), while others have  
191 weaker associations and are found in both *Starships* and non-*Starship* regions across different  
192 strains (e.g., *Gnosis h1*). Variation in the degree to which genes associate with active *Starships*  
193 suggests elements differ in capacity to modulate accessory sequences among strains,  
194 highlighting the importance of investigating *Starships* at the individual element level.

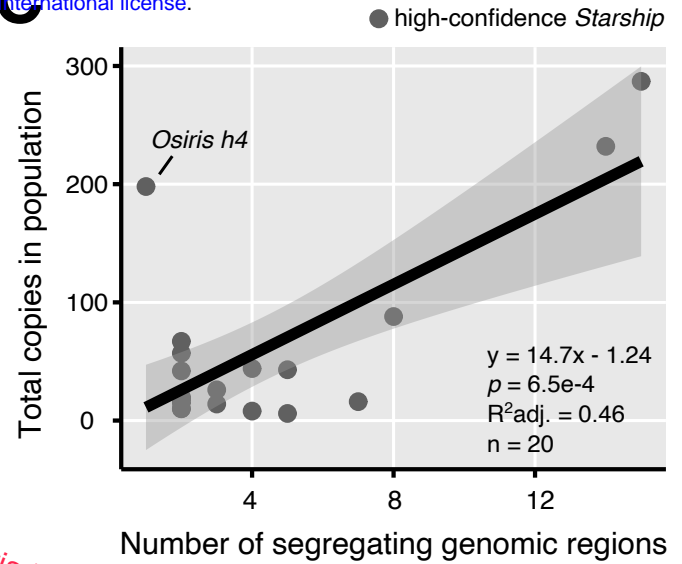
## 195 *Starships* generate structural variation at a genome-wide scale

196  
197 We next asked where *Starship*-mediated variation occurs in the genome to better understand the  
198 implications of *Starship* activity for genome organization. We identified the genomic locations  
199 where *Starships* introduce structural variation by sorting all 787 high and medium-confidence  
200 elements, along with elements detected by BLASTn, into homologous genomic regions (Table  
201 S14, Table S15, Table S16; expanded dataset; Methods). This enabled us to genotype individuals  
202 in the 519 strain population for segregating *Starship* insertions that are polymorphic across strains  
203 (Fig. 3, Fig. S6; Methods). Across all strains and chromosomes, we found 79 regions that contain  
204 at least 1 segregating "empty" insertion site, for a total of 154 sites distributed across all eight  
205 chromosomes (a single region can have >1 insertion site). The average number of empty sites  
206 per genome is 44.5 (range = 9-63, std. dev. = 13.88), indicating that each strain harbors tens of  
207 sites with structural variation introduced by *Starships*. For example, the Af293 reference strain  
208 has a total of 6 full length *Starships* with annotated boundaries and 2 *Starship* fragments, and a  
209 total of 56 segregating empty sites (Fig. 3A). We found a significant linear relationship between  
210 the number of genomic regions a given *Starship* is present in (a proxy for transposition activity)  
211 and the total copy number of that element in the 519 strain population, suggesting active *Starships*

**A**



**C**



**B**

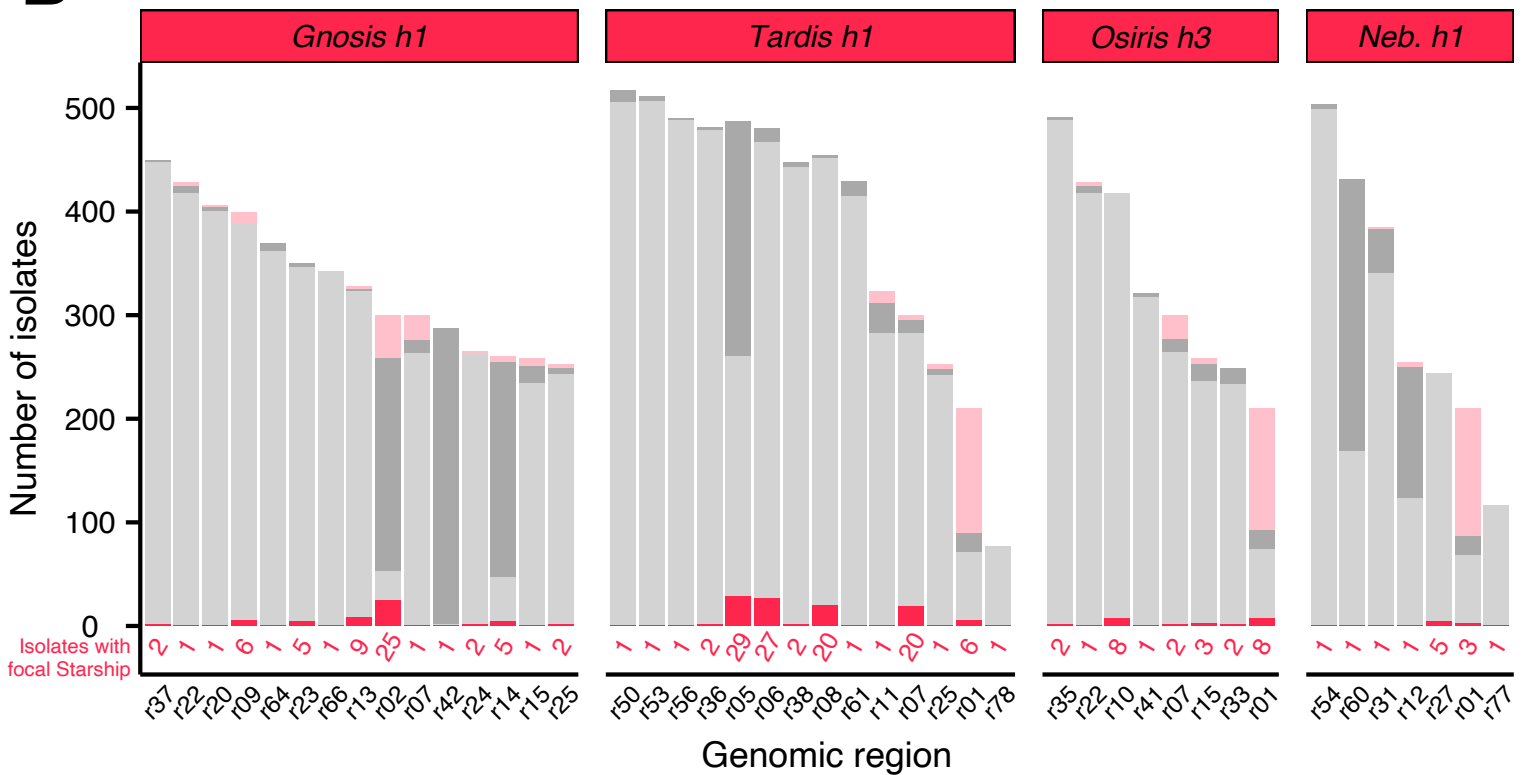


Figure 3: Starships and their insertion sites are distributed across all major chromosomes in the *Aspergillus fumigatus* genome. A) A Circos plot summarizing all inserted Starships (in red) and all genomic regions containing either an empty insertion site or a fragmented Starship (in black, along perimeter and labeled with the r prefix) in the 8 chromosomes of the *A. fumigatus* reference strain Af293 (Table S14). All genomic regions contain a Starship insertion in some other individual from the 519 strain population. B) Barcharts summarizing the genotypes of segregating genomic regions associated with the four most active high-confidence elements in the *A. fumigatus* 519 strain population (Table S16; full dataset in Fig. S6). If an isolate did not have any Starships within a given region, it was assigned either an “empty” or “fragmented” genotype (Methods). C) A scatterplot summarizing the relationship between the number of genomic regions containing a given Starship and the total number of copies of that Starship in the 519 *A. fumigatus* strain population, where each point represents one of the 20 high-confidence Starships. A line derived from a linear regression model is superimposed, with shaded 95% confidence intervals drawn in gray.

212 contribute more to strain heterogeneity compared with less active elements (Fig. 3C;  $y = 14.7x -$   
213  $1.24$ ;  $P = 6.5e^{-4}$ ;  $R^2$  adj = 0.46; expanded dataset).

214

215 Given that *Starships* are mobilized by a site-specific tyrosine recombinase<sup>20</sup>, we attempted to  
216 predict each *Starship*'s target site to gain insight into the genomic sequences that are susceptible  
217 to *Starship* insertions. Among high-confidence *Starships*, 19/20 have identifiable direct repeats  
218 (DRs) ranging from 1-12 bp in length and 18/20 have terminal inverted repeats (TIRs; Table 1,  
219 Table S3). DRs typically reflect a portion of the element's target site, while TIRs are predicted to  
220 facilitate transposition<sup>29</sup>. While precise target site motifs must be confirmed experimentally, the  
221 target site TTACA(N<sub>5</sub>)AAT that we recovered for *Nebuchadnezzar* elements, which belong to the  
222 Hephæstus-family, resembles the canonical *Hephæstus* target site TTAC(N<sub>7</sub>)A, demonstrating  
223 the utility of our approach as a first step towards understanding what sequence features promote  
224 the gain and loss of *Starship*-mediated variation<sup>20</sup>.

225

226 Generally, DRs >6 bp are associated with targeting of the 5S rDNA gene (e.g. *Osiris*), presumably  
227 because this is a relatively stable target site<sup>21</sup>. In contrast to this, *Tardis* has a highly conserved  
228 9 - 11 bp DR that does not correspond to the 5S gene. A k-mer analysis shows that the 10 bp  
229 consensus motif CTACGGAGTA is strongly overrepresented in the genome of Af293 (>99.99th  
230 percentile; Fig. S7), indicating that this motif may represent some other type of highly conserved  
231 genomic sequence, such as a transcription factor binding site. Furthermore, this DR sequence is  
232 conserved among other *Eurotiomycetes*, which could correspond to deep conservation of this  
233 sequence among fungi<sup>21</sup>. This latter result highlights the fact that studying *Starship* elements in  
234 detail can reveal other important aspects of a species' biology, and characterizing the *Tardis* motif  
235 should be of interest for future research.

## 236 *Starships* modulate variation at an idiomorphic biosynthetic gene cluster

237

238 Several genomic regions harbor multiple types of *Starships*, raising the possibility that strain  
239 heterogeneity arises in part from the formation of *Starship* insertion hotspots. We investigated the  
240 genomic region with the highest density of *Starship* insertions to define the upper bounds of  
241 *Starship*-mediated structural variation at a single locus (Fig. 4C, Methods). This region spans an  
242 average of 498.76 Kb (range = 158.07-781.54 kb; std. dev. = 83.02 kb) across the n = 210 strains  
243 for which we could detect it, and ranges from position 584,521-1,108,409 on Chromosome 3 in  
244 the Af293 reference assembly (representing 12.84% of the entire chromosome). By  
245 supplementing starfish's automated genotyping with manual annotation of nine strains with  
246 distinct alleles, we found this region contains at least 7 distinct *Starships* with identifiable DRs and  
247 1 degraded *Starship* that together range from 47.52-151.62 kb long and are inserted into 6  
248 independent segregating sites (Fig. 4C). The majority (75%) of the *Starships* in this region are  
249 inserted into 5S rDNA coding sequences, which effectively fragments that copy of the 5S rDNA  
250 gene. Total 5S rDNA copy number varies between 28-33 in the 13 reference quality assemblies  
251 (median = 31, std. dev. = 1.4; Table S17), but between 6-8 intact copies are typically present at

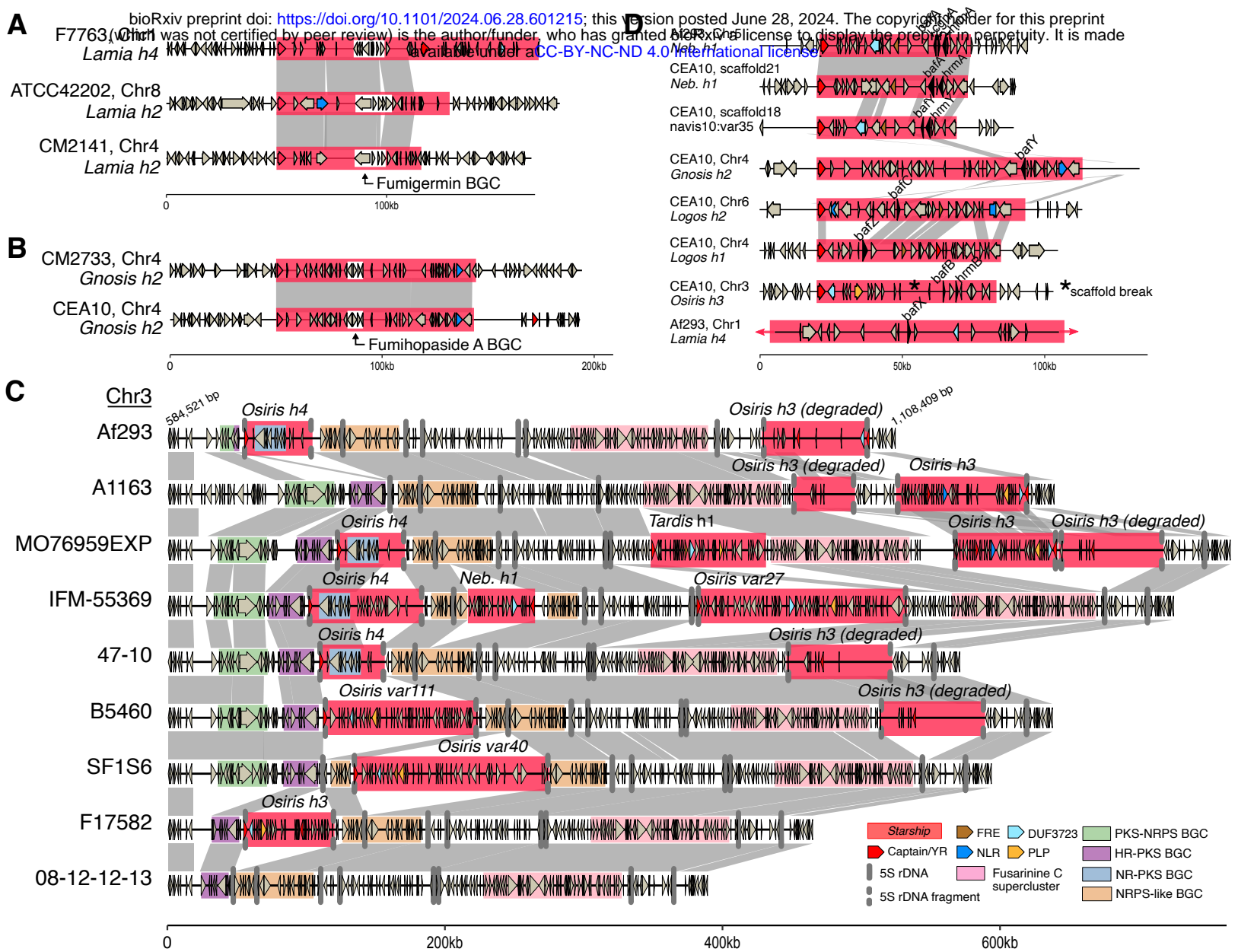


Figure 4: Starships mobilize adaptive traits and generate allelic diversity among *Aspergillus fumigatus* strains. Schematics and alignments of: A) Starship *Lamia h2* and *h4*, which carry the biosynthetic gene cluster (BGC) encoding the polyketide secondary metabolite Fumigermin39, shown inserted at 3 independent sites. B) Starship *Gnosis h2* carrying the BGC encoding the terpene secondary metabolite Fumihopaside A32, shown inserted at 2 independent sites. C) a large region on Chromosome 3 previously identified as an idiomorphic BGC30 containing multiple segregating Starship insertions and various combinations of putative BGCs, including a non-reducing polyketide synthase (NR-PKS) BGC carried by Starship *Osiris h4*. Starships from the *Osiris navis* specifically insert in 5S rDNA sequence and are predicted to fragment it (annotated by two vertical gray bars). D) Eight Starships in the reference strains Af293 and CEA10 that all carry homologs of biofilm architecture factor A (*bafA*)<sup>28</sup>. Starship *Nebuchadnezzar h1* (*Neb. h1*) carries *bafA* as part of the HAAC (*hrmA*-associated gene cluster), while Starship *navis10-var35* carries *bafB* as part of HBAC and Starship *Osiris h3* carries *bafC* as part of HCAC<sup>28</sup>. Only a portion of Starship *Lamia h4* is visualized for figure legibility. All data for A-D was collected from the 519 *A. fumigatus* strain population (Table S5). Links between schematics represent alignable regions  $\geq 5000$ bp and  $\geq 95\%$  nucleotide sequence identity and arrows represent predicted coding sequences. Abbreviations: polyketide synthase (PKS); non-ribosomal peptide synthetase (NRPS); highly reducing (HR).

252 this single locus, representing a ~10-fold enrichment relative to background expectations given  
253 the length of this region (using 5S rDNA frequencies in the Af293 genome). Thus, the enrichment  
254 of 5S rDNA at this locus potentiates *Starship*-mediated variation and the generation of a *Starship*  
255 hotspot.

256  
257 We were surprised to find that in addition to multiple segregating *Starships*, the Chromosome 3  
258 region contains an idiomorphic biosynthetic gene cluster (BGC) that was previously noted to be  
259 a recombination hotspot (Cluster 10 *sensu* Lind et al. 2017)<sup>30,31</sup>. The idiomorphic BGC locus is  
260 polymorphic for upwards of 4 smaller BGC modules and is upstream of a fifth BGC encoding the  
261 biosynthesis of Fusarinine C (BGC8 *sensu* Bignell et al. 2016) that itself is embedded within a  
262 larger stretch of sequence containing NRPS and KR-PKS core genes. While the idiomorphic  
263 modules were not predicted by antiSMASH, manual inspection revealed that each contains a  
264 different core SM biosynthesis gene and numerous other genes involved in metabolic processes,  
265 suggesting they are part of a larger BGC or represent different cryptic BGCs. The NR-PKS BGC  
266 module at this locus is carried by *Starship Osiris h4*, and its presence/absence is directly  
267 associated with the presence/absence of the element, implicating *Starships* as a mechanism  
268 generating idiomorphic BGCs. Furthermore, some BGC modules are disrupted by the insertion of  
269 a *Starship* (e.g., the NRPS-like BGC module). Together, these findings support the assertion that  
270 *Starship* activity generates selectable variation in BGC genotypes. The implication of this variation  
271 for the expression and diversification of natural products warrants further investigation.

## 272 *Starships* encode clinically-relevant phenotypes and are enriched in clinical 273 strains

274  
275 *Starships* encode genes with diverse functions associated with pathogen fitness, including  
276 carbohydrate active enzymes, BGCs and metal detoxification genes (Table 1, Table S5). To  
277 investigate broad trends in how *Starships* might contribute to pathogen phenotypes, we compared  
278 the predicted cargo functions among the 20 high-confidence *Starships* (Table S18; high-  
279 confidence dataset; Methods). As expected, *Starship* types differ from each other in their  
280 predicted functional content, but functional diversity also varies to some extent within elements  
281 from the same type, indicating that both inter- and intra-specific *Starship* variation may contribute  
282 to functional heterogeneity among *A. fumigatus* strains. We found that 49.7% of COG-annotated  
283 genes are “Poorly Categorized”; 28.8% belong to the “Metabolism” category, 14.7% belong to  
284 “Cellular Processes and Signaling” and 6.8% belong to “Information Storage and Processing”.

285  
286 Given the importance of metabolic processes for pathogenicity and overall fitness, we examined  
287 granular classifications within the Metabolism category and found that *Starship* types differ  
288 specifically in their contributions to metabolic heterogeneity (Fig. S8). For example, nearly all 75  
289 copies of *Gnosis h1* carry at least 1 gene with a predicted role in “Coenzyme transport and  
290 metabolism,” and none carry genes with predicted roles in “Lipid transport and metabolism”, while  
291 the exact opposite is true for the 119 copies of *Tardis h1*. The most frequently mobilized COG

292 metabolism categories are “Carbohydrate transport and metabolism” (present in 371 individual  
293 elements belonging to 13 high-confidence *Starships*), “Secondary metabolite transport and  
294 metabolism” (present in 329 elements belonging to 16 high-confidence *Starship* types) and  
295 “Energy production and conversion” (present in 281 elements belonging to 9 high-confidence  
296 *Starship* types), each of which has known associations with clinically-relevant pathogen  
297 phenotypes.

298  
299 While investigating associations between *Starships* and characterized pathogen phenotypes, we  
300 found three notable examples of cargo genes that encode known traits important for pathogen  
301 survival and virulence (Table S19, Methods)<sup>9,10,30,32–38</sup>. The BGC encoding Fumihopaside A  
302 (AFUA\_5G00100-00135) is carried by *Starship Gnosis h2* (Fig. 4A). Fumihopaside A is a  
303 triterpenoid glycoside that increases fungal spore survival under heat and UV stress exposure<sup>32</sup>.  
304 Similarly, the BGC encoding the polyketide Fumigermin (AFUA\_1G00970-01010), which inhibits  
305 bacterial spore germination, is carried by *Lamia h2* and *h4* (Fig. 4B)<sup>39</sup>. Both the Fumigermin and  
306 Fumihopaside A BGCs were previously identified as “mobile gene clusters” based on their  
307 presence/absence at different chromosomal locations in *A. fumigatus* strains, and our results  
308 reveal that *Starships* are the mechanism underpinning their mobility (Cluster 1 and 33,  
309 respectively from Lind et al., 2017)<sup>30</sup>. Finally, a cluster of three genes (AFUA\_5G14900/*hrmA*,  
310 AFUA\_5G14910/*cgnA*, AFUA\_5G14915/*bafA*, collectively referred to as the *hrmA*-associated  
311 cluster or HAC) carried by *Nebuchadnezzar h1* increases virulence and low oxygen growth, and  
312 its expression modulates colony level morphological changes associated with biofilm  
313 development (Fig. 4D)<sup>28,40</sup>. The genes *bafB* and *bafC*, which are homologs of *bafA*, also determine  
314 colony and submerged biofilm morphology and are each carried by up to 5 additional *Starships*,  
315 indicating a sustained association between this gene family and *Starships* (Fig. 4D, Fig. S9)<sup>28</sup>.  
316 Mobilization within and between genomes likely contributes to the rapid evolution of these survival  
317 and virulence traits through the processes of gene gain and loss, effectively increasing the  
318 capacity of these traits to evolve in populations. We propose that by mobilizing these genes,  
319 *Starships* drive heterogeneity in clinically-relevant phenotypes<sup>28</sup>.

320  
321 To identify more *Starships* that could be relevant in clinical settings, we tested for an association  
322 between the high-confidence *Starships* and strain isolation source (genotyping dataset; Methods).  
323 We found that 5 high-confidence *Starships* are significantly enriched ( $P_{\text{adj}} < 0.05$ ) in strains from  
324 either clinical or environmental isolation sources across the 475/479 genotyped strains for which  
325 source data exists (Table S2, Table S20, Fig. S10). *Lamia h3* ( $P_{\text{adj}} = 0.013$ ) and *Janus h3* ( $P_{\text{adj}} =$   
326  $0.034$ ) are enriched in environmental strains, while *Osiris h4* ( $P_{\text{adj}} = 0.022$ ), *Nebuchadnezzar h1*  
327 ( $P_{\text{adj}} = 0.015$ ; carries *bafA*, see above) and *Janus h2* ( $P_{\text{adj}} = 0.013$ ) are enriched in clinical strains.  
328 Although we can't completely rule out biases in our sampling that would contribute to these  
329 enrichment patterns, strains with these 5 *Starships* were isolated from different countries  
330 (between 3-10) and belong to different phylogenetic groups (between 1-3 clades sensu Lofgren  
331 et al., 2022 and 1-6 phylogenetic clusters sensu Barber et al., 2021). Further investigation is  
332 necessary to test how these particular *Starships* contribute to fitness in non-clinical and clinical  
333 settings.

334 *Starship* expression contributes to heterogeneity in a strain-, treatment- and  
335 strain by treatment-dependent manner

336

337 The revelation of *A. fumigatus*' *Starships* allowed us to re-examine RNA-seq datasets available  
338 for this pathogen to test the hypothesis that *Starship* cargo is expressed under clinically-relevant  
339 conditions. We analyzed patterns of differential *Starship* cargo gene expression using 14  
340 transcriptomic studies with easily comparable treatments from three commonly used reference  
341 strains (Af293, CEA10, A1163), for a total of 177 samples. We identified 459 differentially  
342 expressed genes (DEGs) in *Starships* across the three reference strains (Supplementary Data),  
343 out of 596 *Starship* genes total. We did not find a significant enrichment of DEGs within *Starships*  
344 compared to the genomic background of any strain (Fisher's Exact Test  $P$ -values  $> 0.05$ ).  
345 However, we found that *Starship* DEGs vary across element naves, fungal strains, and  
346 experimental conditions, indicative of pervasive strain-specific, treatment-specific and strain by  
347 treatment interactions impacting *Starship* cargo expression (Fig. 5B & Fig. S13).

348

349 To identify experimental conditions that may impact *Starship* transposition and the subsequent  
350 generation of *Starship*-mediated heterogeneity, we examined patterns of transcript abundance  
351 for captain genes responsible for *Starship* transposition within 12 high-confidence *Starships* from  
352 the reference strains Af293 (Fig. 5A), CEA10 and A1163 (Fig. S11). All captain genes have  
353 evidence for constitutive gene expression (a minimum median transcript coverage of 1 across the  
354 gene body for biological replicates) in at least one experimental condition (Fig. S12). Overall, 8 of  
355 the 12 captain genes from high-confidence *Starships* are differentially expressed in at least one  
356 study for one or more reference strains, revealing myriad conditions that create opportunities for  
357 *Starship* transposition (Supplemental information). Differences in experimental conditions and/or  
358 strain backgrounds have no consistent positive or negative influence on captain gene expression,  
359 indicating that the intricacies of captain expression remain to be elucidated (Fig. 5B).

360

361 We then examined patterns of differential expression for *Starship*-mobilized cargo genes in order  
362 to identify conditions where *Starships* have potential to impact organismal phenotypes. As with  
363 captain genes, the expression of cargo genes is context-dependent, with strain background,  
364 experimental condition and *Starship* *haplotype* impacting gene transcription (Fig. 5B). For  
365 example, we compared transcript abundance patterns for genes within the *hrmA*-associated  
366 cluster (HAC) between treatment categories and found that the transcription of genes in the HAC  
367 appear to be down-regulated in select infection environments (Fig. 5A & Figure S11). Together,  
368 strain identity, treatment conditions, and non-additive interactions between strains and treatments  
369 generate variation in *Starship* cargo expression.

370

371 To gain further insight into *Starship*-mediated heterogeneity in gene expression and regulation,  
372 we built weighted gene co-expression networks (WGCNA) that capture correlations between gene  
373 expression patterns to reveal the broader regulatory network of the cell. We identified five  
374 modules as being significantly associated with "antifungal"-, "infection"-, or "nutrient"-based

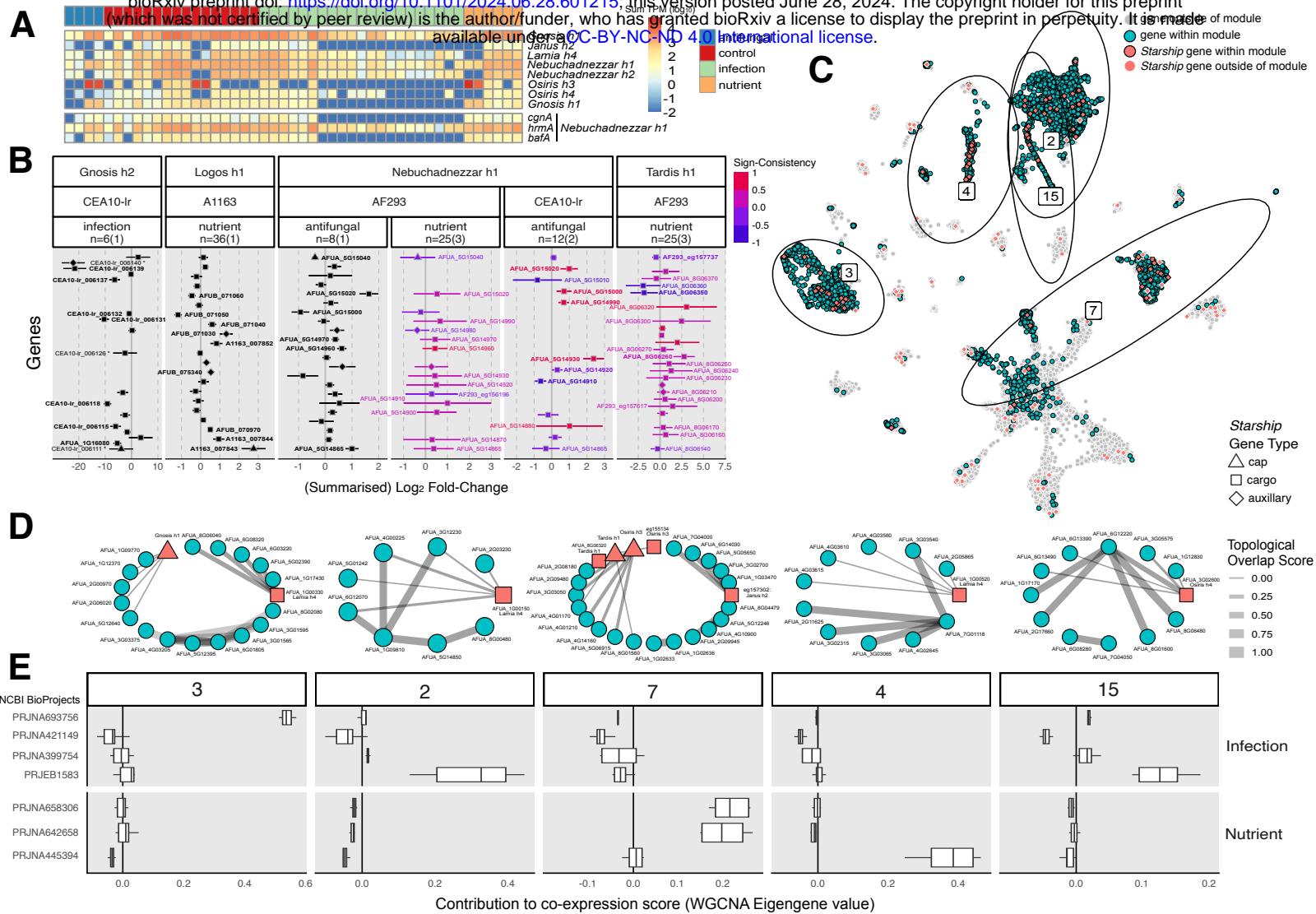


Figure 5: A) A heatmap of transcript abundances (log<sub>10</sub>TPM) of Starship captain tyrosine recombinase genes (top) and genes within the hrmA-associated cluster (HAC; bottom), collapsed across treatment replicates, for 11 RNAseq studies from *A. fumigatus* Af293. B) Results from differential expression (DE) tests for select Starships, treatment categories, and strain combinations. Only genes with valid output from DE tests are shown, and only genes with significantly DE are labeled with gene codes. Genes with extreme count outliers, as determined by Cook's Distance in DESeq2, do not have valid p-values and are labeled with an asterisk ("\*"). DE based on a single study are shown as log<sub>2</sub> fold-change (log<sub>2</sub>FC) in black with standard error bars, whereas DE genes identified across multiple studies are represented with summarized log<sub>2</sub>FC values from a random effects model (REM) and coloured by "sign-consistency", the number of studies that reported DE in the positive (+1) or negative (-1) direction, centered around 0. Labels in bold font represent DEGs that are significantly DE in more than one study. C) The results of a weighted gene co-expression network analysis (WGCNA) constructed from 14 "antifungal", "infection", and "nutrient" RNAseq studies represented using UMAP clustering based on the co-expression eigengene values for all genes in the *A. fumigatus* Af293 genome. Non-Starship genes present within modules of interest are shown in blue, while all Starship genes are shown in red, with those genes within modules of interest having a black outline. D) Genes within modules that were significantly associated with samples from specific treatment categories or studies were used to construct sub-networks which contained the top 10 edges in the network that were made between any pair of genes or any gene and a Starship captain. The connections between genes (edges) are based on the topological overlap matrix (TOM) for each module, and have been 0-1 scaled. E) Boxplots of eigengene values from WGCNA, akin to a weighted average expression profile, indicate the extent of co-expression (correlation) of the genes present within each module. Pairwise comparisons of module eigengene values determined if a module was significantly associated with samples from specific treatment categories or studies (Fig. S15).

375 studies (Fig. 5E). We identified two major trends in the transcriptional network properties of  
376 *Starship* cargo. First, we found multiple *Starship*-associated genes that integrate into modules  
377 containing numerous background genes, underscoring the possibility that phenotypes emerging  
378 from these networks are the product of regulatory interactions between *Starship* and non-*Starship*  
379 genes (Fig. 5D & Fig. S14). Connections involving captains in particular further highlight candidate  
380 loci involved in regulatory interactions between *Starships* and the *A. fumigatus* genome, and are  
381 prime targets for future investigations of the gene networks involved in *Starship* transposition (Fig.  
382 5E). Second, we also identified modules composed of mainly *Starship* cargo, indicative of modular  
383 networks specific to particular *Starships*. These network analyses paint a nuanced picture of how  
384 *Starships* interact with the broader transcriptional networks of the cell, and implicate the  
385 expression of *Starship* cargo in the generation of transcriptional variation.

## 386 Discussion

387  
388 Phenotypic heterogeneity among fungal pathogen strains poses a major challenge for combating  
389 infectious diseases, yet little is known about the genetic basis of this variation. We hypothesized  
390 that a newly discovered group of unusual MGEs, *Starships*, would be major drivers of strain  
391 heterogeneity. We tested this hypothesis by systematically characterizing *Starship* activity and  
392 expression in *A. fumigatus*, an important human fungal pathogen of critically high research  
393 priority<sup>1,41</sup>. Our work provides foundational insight into the mode and tempo of fungal evolution by  
394 revealing that strain variation emerges not only from single nucleotide or copy number variation  
395<sup>9,10</sup> but from the previously hidden activity of giant transposons.

396  
397 Although much remains unknown about the fundamentals of *Starship* biology, *Starships* in *A.*  
398 *fumigatus* likely generate variation on a scale approaching MGE-mediated evolution in bacteria,  
399 which is a major mechanism driving bacterial adaptation. The median number of *Starship*-borne  
400 genes per *A. fumigatus* isolate is 0.8% (range = 0 - 2.1%), while between 2.9-4.8% of the  
401 pangenome (corresponding to between 9.7-16% of the accessory genome) is *Starship*-  
402 associated. These observations approach analogous measurements of bacterial plasmids in the  
403 Enterobacteriaceae, where the median number of plasmid-borne genes per genome is estimated  
404 at 3.3% (range = 0 - 16.5%) and where between 12.3 - 21.5% of the pangenome is plasmid-  
405 associated<sup>42</sup>. Given our strict requirements that a high-confidence *Starship* be found in 2 different  
406 locations in 2 different strains, our estimates represent a conservative assessment of the mobile  
407 fraction of *A. fumigatus*' genome. Mobility underpins prokaryotic genome dynamics, yet current  
408 models of fungal pathogen physiology and evolution do not take gene mobility into account. These  
409 data highlight the need to understand the population level impacts of *Starships* across a larger  
410 number of plant and animal pathogen species and to integrate these findings into a new predictive  
411 framework for fungal pathogenesis. Our *Starship* atlas thus provides practical insights for  
412 elucidating *A. fumigatus* pathobiology and establishes a roadmap for deciphering the origins of  
413 strain heterogeneity across the fungal tree of life.

414

## 415 Online Methods

### 416 Long-read genome sequencing, assembly and annotation

417  
418 For DNA extraction strains were grown at 37 °C for 24 hours in shaking liquid cultures using 1%  
419 glucose minimal media<sup>43</sup>. Biomass was collected by gravity filtration through Miracloth (Millipore).  
420 High molecular weight DNA extraction followed the Fungal CTAB DNA extraction protocol<sup>44</sup>.  
421 Biomass was ground in liquid nitrogen and incubated at 65 °C in a lysis buffer composed of 650  
422 µl of Buffer A (0.35 M sorbitol, 0.1 M Tris-HCl pH 9, 5 mM EDTA pH 8), 650 µl Buffer B (0.2 M  
423 Tris-HCl pH 9, 0.05 M EDTA pH8, 2M NaCl, 2% CTAB), 260 µl of Buffer C (5% Sarkosyl), 0.01%  
424 PVP, 0.2 mg proteinase K for 30 minutes. Potassium acetate (280 µl of 5M solution) was added  
425 and incubated on ice for 5 minutes. DNA was extracted by phenol:chloroform:isoamyl alcohol  
426 extraction followed by a secondary extraction with chloroform:isoamyl alcohol. The supernatant  
427 was RNase treated (2.5µg), and precipitated using sodium-acetate( 0.3M) and isopropanol. DNA  
428 was finally purified using 70% ethanol, dried and rehydrated in TE (pH 9). To preserve long  
429 strands of DNA suitable for long-read sequencing samples were gently mixed by inversion and  
430 transferred using large bore pipette tips. DNA quality was assessed using NanoDrop and  
431 concentration quantified using Qubit dsDNA BR assay kit. Finally DNA fragment size was  
432 assessed on 1% agarose gel, looking for large quantities of DNA to remain in the well after 1 hour  
433 of running at 100v. DNA was sent to SeqCoast for Oxford Nanopore Sequencing. We used  
434 previously sequenced Illumina short read data for polishing the assemblies with Pilon<sup>9</sup>. Two  
435 strains not previously sequenced were sequenced with Illumina at SeqCoast.

436  
437 The long-read genome assemblies were assembled with Canu v2.2 and polished with five rounds  
438 of Pilon v wrapped with AAFTF v0.3.0<sup>45-47</sup>. Summary statistics for each assembly were computed  
439 with AAFTF and BUSCO using eurotiomycetes\_odb10 marker set<sup>48</sup>. Genome annotation was  
440 performed using Funannotate v1.8.10 which trained gene predictors with PASA using RNA-Seq  
441 generated for each strain (Puerner et al., forthcoming), and predicted genes de novo in each  
442 assembly and produced a consensus gene prediction set for each strain<sup>49,50</sup>.

### 443 Functional predictions

444  
445 We annotated all predicted genes with Pfam domains, InterPro domains and GO terms using  
446 InterproScan v5.61-93.0 (-appl Pfam --iprlookup --goterms)<sup>51</sup>. We annotated carbohydrate active  
447 enzymes using dbcan v3.0.4 (--tools all) and EggNOG orthogroups and COG categories using  
448 eggno-mapper v2.1.7 (--sensmode very-sensitive --tax\_scope Fungi)<sup>52,53</sup>. We annotated  
449 biosynthetic gene clusters using antiSMASH v6.0.1 (--taxon fungi --clusterhmmmer --tigfam) and  
450 5S rDNA using infernal v1.1.4 (--rfam -E 0.001)<sup>54,55</sup>. On average, 35.7% of genes within *Starships*  
451 have no known PFAM or Interpro domain, GO term, COG category or eggNOG orthology (range  
452 = 0-67.6%, std. dev. = 14.8%) but approximately half of all mobilized genes could be assigned to

453 a COG (e.g., 50% of 11,900 genes total, across 459 high-confidence elements). To investigate  
454 associations between *Starships* and pathogen phenotypes, we searched for the presence of 798  
455 genes known to be associated with virulence or infection-relevant phenotypes on *Starships* (Table  
456 S19, Methods)<sup>9,10,30,32–38</sup>.

457

## 458 SNP analysis

459 We calculated pairwise kinship among strains by analyzing a previously generated VCF of all  
460 high-quality, filtered, biallelic single nucleotide polymorphisms (SNPs) from the Lofgren et al. 2022  
461 population with plink (--distance square ibs flat-missing --double-id --allow-extra-chr; Fig. 1E)<sup>56,57</sup>.  
462 We calculated Jaccard similarity in *Starship* repertoire among all pairwise combinations of strains  
463 using genotyping data for the set of 20 high-confidence *Starships* and the following formula:  
464  $\text{Starships shared between strain 1 and 2} / (\text{Starships unique to strain 1} + \text{Starships unique to}$   
465  $\text{strain 2} + \text{Starships shared between strain 1 and 2})$ .

466

## 467 Pangenome construction

468 We constructed a pangenome for all 519 strains using Orthofinder (--only-groups -S diamond),  
469 and then extracted all orthogroups containing at least 1 of the 13 reference-quality strains for  
470 analysis (Fig. 2B)<sup>58</sup>. Core orthologs are defined as being present in all 13 strains; accessory  
471 orthologs are present in between 2-12 strains; singleton orthologs are present in 1 isolate. We  
472 included all 519 strains in the Orthofinder analysis to ensure that ortholog groups are consistent  
473 across different population subsets.

## 474 BLAST analysis

475 We determined the genomic locations of all best reciprocal blast hits to cargo genes carried by  
476 the 20 high-confidence *Starships* using BLASTp (Fig. 1C)<sup>59</sup>. For each cargo gene, we retrieved  
477 the highest scoring hit with  $\geq 90\%$  identity and  $\geq 90\%$  query coverage in each of the 13 reference-  
478 quality assemblies, and determined whether that hit was found in the same *Starship*, a different  
479 *Starship*, or not in a *Starship* at all. If no hit was retrieved, that gene was marked as missing.

480

## 481 Structural variant analysis

482 To evaluate the validity of putative structural rearrangements within our CEA10-Ir assembly, we  
483 took two approaches. First, we aligned the raw nanopore reads to the CEA10-Ir assembly using  
484 Mummer 4.0 with the nucmer command and default parameters<sup>60</sup>. Alignments were then visually  
485 inspected using the Genome Ribbon software<sup>61</sup>. This method confirmed that individual reads  
486 spanned the junctions of putative rearrangements and confirmed that no misassemblies were  
487 present. However, this approach suggested that two alternative chromosomal topologies existed:  
488 one that matches the chromosomal assemblage of the reference strain Af293, and another that  
489 exhibits a reciprocal translocation between Chromosomes 1 and 6, as reported for other  
490 assemblies of CEA10<sup>62</sup>. To resolve this paradox, we then mapped the raw nanopore reads to

491 both the CEA10-Ir assembly, as well as a publicly available high-quality assembly (BioSample:  
492 SAMN28487501) with the minimap2 map-ont command<sup>63</sup>. These were then visually inspected  
493 using the IGV genome browser<sup>64</sup>. Multiple reads support both topologies, implying that the  
494 CEA10-Ir isolate sequenced here is a heterogeneous mix of at least two lineages derived from  
495 the same CEA10 ancestor, likely obscuring estimates of the frequency with which *Starships* are  
496 mobilizing. Additionally, we examined the location of the annotated *Starship* elements, which for  
497 many elements revealed multiple reads where the given *Starship* was absent, suggesting that the  
498 element had either excised itself when mycelia was cultured for DNA extraction, or that additional  
499 derived lineages with variation at these loci were present in the sample. To resolve these  
500 possibilities, single conidial strains will have to be obtained and resequenced.

501  
502 To further assess whether *Starships* transpose frequently enough to generate variation among  
503 isolates of the same strain, we evaluated three additional strains that we sequenced with  
504 Nanopore long-read technology that also had publicly available short-read data generated by  
505 other research groups: ATCC46645-Ir, S02-30, and TP9. Short-read sequence data were mapped  
506 to our long-read assemblies and visually inspected in IGV to determine if any *Starships* were  
507 deleted/transposed in the public data. Both S02-30 and TP9 had no apparent variation at *Starship*  
508 loci. However, ATCC46645-Ir showed polymorphism at three *Starships*, namely *Nebuchadnezzar*  
509 h1, *Nebuchadnezzar* h2, and *Gnosis* h1, indicative of active transposition. Both of the  
510 *Nebuchadnezzar haplotypes* show clean deletions, indicating that they may have jumped out of  
511 the genome of some nuclei within a particular isolate, while the deletions around *Gnosis* (5 in  
512 total) were more complex, which may be a signature of genomic instability rather than *Starship*  
513 mobilization. Note that neither S02-30 nor TP9 have *Nebuchadnezzar h1*.

## 514 *Starship* annotation

515 We systematically annotated *Starships* in the 12 newly sequenced long-read genomes plus 507  
516 publicly available *A. fumigatus* genomes by applying the starfish workflow v1.0.0 (default settings)  
517 in conjunction with metaeuk, mummer4, CNEFinder and BLASTn (Table S2)<sup>21,59,60,65,66</sup>. Briefly,  
518 captain tyrosine recombinase genes were *de novo* predicted with starfish's Gene Finder Module  
519 and full length elements associated with captains were predicted with starfish's Element Finder  
520 Module using pairwise BLAST alignments to find empty and occupied insertion sites. We filtered  
521 out all elements that were <15kb in length, which we have found to correspond to indels of captain  
522 genes but never to the transposition of a full length *Starship*. We then manually examined  
523 alignments between each putative *Starship* and its corresponding insertion site, and filtered out  
524 all "low confidence" poorly supported alignments indicative of a false positive insertion. Poor  
525 alignments were observed most often when *Starships* inserted into smaller transposons; when an  
526 inversion breakpoint occurred within a putative *Starship*, resulting in an over-estimation of  
527 *Starship* length; or when the insertion site was on a very small contig resulting in small flanking  
528 region alignments.

529

530 We verified and supplemented these automated *Starship* predictions with manual annotations of  
531 the 3 reference strains Af293, CEA10 and A1163, along with a set of 86 additional elements  
532 (Table S7, Table S3). Insertion sites and DRs were manually verified by generating alignments of  
533 the elements plus the 50kb flanks to a corresponding putative insertion site, as determined by  
534 starfish (Table S4). MAFFT was used to generate alignments with default parameters<sup>67</sup>. The DRs  
535 were visually assessed and the insertion regions were examined for the presence of TEs, which  
536 could lead to erroneous target site, DR and TIR determinations. For *Starships* in the three  
537 reference genomes, the set of reference *Starships* was used as a query with BLAST to verify their  
538 start and end coordinates, and insertion sites. Additionally, the starfish output was examined for  
539 additional elements which did not meet our initial strict cutoffs to attempt to capture the entire  
540 *Starship* repertoire of these strains.

### 541 *Starship* classification

542 *Starships* were then grouped into *naves* (singular: *navis*, latin for “ship”) by clustering captain  
543 sequences in ortholog groups using mmseqs easy-cluster (--min-seq-id 0.5 -c 0.25 --alignment-  
544 mode 3 --cov-mode 0 --cluster-reassign)<sup>68</sup>. *Starship* sequences were then grouped into  
545 *haplotypes* using the MCL clustering algorithm in conjunction with sourmash sketch (-p k=510  
546 scaled=100 noabund) that calculated pairwise k-mer similarities over the entire sequence length,  
547 as implemented in the commands “starfish sim” and “starfish group”<sup>69,70</sup>. These automated and  
548 systematic predictions yielded a core set of 787 individual elements grouped into 54 distinct *navis*-  
549 *haplotype* combinations.

550  
551 We identified segregating insertion sites associated with the 787 elements across all 519 strains  
552 using the command starfish dereplicate (--restrict --flanking 6 --mismatching 2) in conjunction with  
553 the Orthofinder orthogroups file (see above) that was filtered to contain groups absent in at most  
554 517 strains and present in at most 8 copies per isolate. Starfish dereplicate enables the  
555 identification of independently segregating insertions by grouping *Starships* and their insertion  
556 sites into homologous genomic regions using conserved combinations of orthogroups between  
557 individuals. We genotyped the presence of each *navis-haplotype* combination within each region  
558 for each isolate. If an isolate did not have any *Starships* within a given region, it was assigned  
559 either an “empty” genotype (if the set of orthogroups that define the upstream region flank were  
560 adjacent to the set of orthogroups that define the downstream region flank) or a “fragmented”  
561 genotype (if additional orthogroups were in between the upstream and downstream region flanks).

562  
563 To define high-confidence *Starships*, we used a conservative threshold that required observing  
564 the same *navis-haplotype* in  $\geq 2$  independent segregating sites in different strains, which ensured  
565 an accurate and precise determination of each element’s boundaries and the sequences  
566 therein<sup>21</sup>. We found 18 *navis-haplotype* combinations meeting these criteria. We considered 2  
567 additional *navis-haplotype* combinations of interest (*Osiris h4* and *Lamia h4*) to be high-  
568 confidence after manually annotating their boundaries and finding evidence for flanking direct

569 repeats that are signatures of *Starship* boundaries. Each high-confidence *Starship* is represented  
570 by a type element (similar in concept to a type specimen for defining a biological species) that  
571 constitutes the longest element assigned to that *navis-haplotype*. The type elements of the  
572 reference *Starships* range in size from 16,357-443,866 bp, and collectively represent 459  
573 individual elements with an average length of 71,515 bp (Table S4, Table S5). The remaining 328  
574 elements have an average length of 50,249 bp and are represented by 34 “medium-confidence”  
575 *navis-haplotypes* that were only observed at a single segregating site. We predicted the target  
576 sites of each high-confidence *Starship* by manually aligning multiple empty insertion site  
577 sequences to each other and identifying columns within 25bp of the core motif that had conserved  
578 nucleotides in at least 80% of sequences (Table 1).

579  
580 Each *navis* associated with a high-confidence element was assigned a charismatic name (e.g.,  
581 *Tardis*) and a new, sequentially named *haplotype* (*h1*, *h2*, etc.) to distinguish it from the  
582 automatically generated *haplotype* codes (*var14*, *var09*, etc.). All other 34 *navis-haplotype*  
583 combinations with evidence of only a single segregating site were classified as “medium-  
584 confidence”. Medium-confidence *Starships* with captains not belonging to the high-confidence  
585 naves kept their automatically generated *navis* and *haplotype* codes (e.g., *navis01-var09*), while  
586 medium-confidence *Starships* with captains belonging to the high-confidence naves were  
587 assigned to that *navis* but kept their automatically assigned *haplotype* (e.g., *Osiris-var04*).

## 588 *Starship* genotyping

589 *Starfish* requires a well-resolved empty insertion site in order to annotate the boundaries of a  
590 contiguous *Starship* element. It will therefore not annotate any element whose corresponding  
591 empty site is missing, or any element that is partially assembled or not assembled at all. We  
592 therefore supplemented *starfish* output using a combination of BLASTn and short-read mapping  
593 to decrease the false negative rate for presence/absence genotyping. First, we recovered full  
594 length and partial elements using the set of high-confidence *Starships* as input to the command  
595 “*starfish extend*”. This command uses BLASTn to align full length *Starship* elements to the  
596 sequence downstream from all tyrosine recombinase genes not affiliated with a full length  
597 *Starship* element.

598  
599 Separately, we downloaded paired-end short read Illumina sequencing data for all 466 strains for  
600 which these data were available and mapped them to the 20 high-confidence *Starships* using the  
601 command “*starfish coverage*” and the aligner *strobealign*<sup>71</sup>, ensuring that we would correctly  
602 genotype the presence/absence of a *Starship* even if it is not present in an assembly or partially  
603 assembled. We considered any *Starship* with a minimum of 5 mapped reads at each position  
604 across 95% of its entire length to be present. We considered a *Starship* to be present in a given  
605 individual if either the main *starfish* workflow, BLASTn extension, or short-read mapping identified  
606 it as present; otherwise we considered it absent.

607

## 608 *Starship* datasets

609 We explored a variety of methods for predicting *Starships*, including manual and automated  
610 annotation, BLAST-based detection, and read-mapping to a known *Starship* library (see above).  
611 Certain detection methods were more appropriate for particular analyses, resulting in the  
612 partitioning of our findings into three datasets: the high-confidence dataset, expanded dataset,  
613 and genotyping dataset. To analyze *Starship* features, like gene content and pangenome  
614 distributions, we took a conservative approach by limiting our analyses to the set of 459 high-  
615 confidence elements for which we have end-to-end boundaries and evidence of transposition  
616 (high-confidence dataset). For analyses that examine the presence/absence of elements across  
617 all genomic regions, we used an expanded set of 1818 elements that consists of the 787 high and  
618 medium-confidence elements as well as 1031 elements whose presence was detected through  
619 BLAST searches (i.e., with starfish ‘extend’ boundaries’), because these methods maximize our  
620 ability to correctly predict the presence/absence of an element in a given region (expanded  
621 dataset; Table S4, Table S5). For genotyping analyses that focus on detecting the  
622 presence/absence of an element regardless of where it is found in the genome, we took an even  
623 more conservative approach by limiting our analysis to the 13 reference quality assemblies plus  
624 466 *A. fumigatus* strains with paired-end short-read Illumina sequencing data that were used to  
625 validate *Starship* presence/absence with short-read mapping (genotyping dataset; Table S21).

## 626 Meta-Analysis of *A. fumigatus* RNAseq Datasets

627 We collected transcriptomes from a total of 434 paired-end libraries of *A. fumigatus* strains Af293,  
628 A1163, and CEA10/CEA17. We surveyed the available metadata from each BioProject and  
629 binned the samples into general categories based on the type of treatment applied in each study.  
630 The categories that were the most well represented across multiple BioProjects include exposure  
631 to antifungals (“antifungal”), *in vivo* and *in vitro* infection experiments (“infection”), or  
632 supplemented growth media with specific nutrients (“nutrient”; Table S22, Table S23).

633  
634 RNAseq reads were retrieved from the NCBI SRA using *fasterq-dump* from the SRA toolkit (last  
635 accessed June 26, 2024: <https://github.com/ncbi/sra-tools>) and were trimmed for quality and  
636 sequencing artifacts using *TrimGalore* (last accessed June 26, 2024:  
637 <https://github.com/FelixKrueger/TrimGalore>). Transcripts were quantified using *salmon quant*,  
638 which employs a reference-free pseudo-mapping based approach to quantify transcripts. In  
639 addition to the pseudo-BAM files created by *salmon*<sup>72</sup>, we created separate sets of BAM files to  
640 assess transcript coverage across *Starship* genes by mapping to the transcriptome with *STAR*<sup>73</sup>.  
641 We assessed transcript coverage across the core of *Starship* genes using the *bamsignals* R  
642 package (last accessed June 26, 2024: <https://github.com/lamortenera/bamsignals>). Genes with  
643 a median core-transcript coverage less than 1 were considered to have insufficient evidence of  
644 being expressed. We applied an abundance filter on transcript abundances, removing genes  
645 represented by fewer than 10 transcripts in at least 3 samples. We corrected for batch effects  
646 between BioProjects using *CombatSeq*<sup>74</sup> and excluded BioProjects with inconsistent/unclear  
647 metadata, or those that remained as outliers in the PCA after batch-correction. *DESeq2*<sup>75</sup> was

648 used to perform a series of differential expression (DE) using the corrected transcript counts.  
649 These DE tests were performed individually for each BioProject, DE tests compared the  
650 differences in expression between all control and treatment samples in each BioProject, including  
651 treatment level as a cofactor in the model, where applicable.

652  
653 To summarize expression patterns across BioProjects which tested similar conditions, we  
654 employed a random effects model (REM) using the R package *metaVolcanoR*<sup>76</sup>. This method  
655 identifies differentially expressed genes (DEGs) as genes that are significantly differentially  
656 expressed in all studies and accounts for the variation in the expression for each DEG observed  
657 in multiple BioProjects. The output from the meta-volcano REM are summarized log<sub>2</sub> fold-change,  
658 a summary p-value, and confidence intervals for each DEG. In addition, a measure of “sign-  
659 consistency” is used to evaluate the consistency of DEG, which is expressed as a count of the  
660 number of BioProjects where a DEG was observed with the same directional change (+/-),  
661 centered around 0.

662  
663 We performed weighted gene co-expression network analysis (WGCNA) using *PyWGCNA*<sup>74</sup> to  
664 construct gene co-expression networks for *A. fumigatus* reference strain Af293. A single network  
665 was constructed using the batch-corrected TPM values from the collection of samples belonging  
666 to “antifungal”, “infection”, and “nutrient” treatment categories. *PyWGCNA* automatically  
667 estimates an appropriate soft-power threshold based on the lowest power for fitting scale-free  
668 topology and identifies modules of co-expressed genes through hierarchical clustering of the  
669 network and performing a dynamic tree cut based on 99% of the dendrogram height range. The  
670 topological overlap matrix is then computed and a correlation matrix is constructed to produce the  
671 final network. Distributions of TOM scores were generated based on edges in the network  
672 between genes within *Starships*, between *Starships*, between *Starships* and the rest of the  
673 genome, and between non-*Starship* genes in the genome. We compared these distributions using  
674 a Wilcoxon test and anova, adjusting p-values with the Holm–Bonferroni method. Modules in the  
675 network that were significantly associated with samples from a specific treatment category were  
676 identified using the pairwise distances between observations using *pdist* from the python module  
677 *scipy*<sup>77</sup>. To highlight the genes within each module that have the most strongly correlated  
678 expression profiles, sub-networks were constructed using only the edges 10 highest TOM scores  
679 made between either *Starship* captain genes or any non-*Starship* gene that was present in the  
680 module. The collections of genes within these modules were also tested for functional enrichment  
681 using *gprofiler2*<sup>78</sup>.

## 682 Statistical tests and data visualization

683 Enrichment tests were performed with either the Binomial test (`binom.test`; alternative = “greater”)  
684 or the Fisher’s exact test (`fisher.test`; alternative = “greater”) implemented in base R, using the  
685 `p.adjust` function (method = Benjamini-Hochberg) to correct for multiple comparisons. We  
686 visualized all element alignments and insertion site distributions using *circos* and *gggenomes*<sup>79,80</sup>.  
687 All other figures were generated in R using *ggplot2*<sup>81</sup>.

## 688 Data availability

689 Sequencing reads and genomic assemblies for the 12 isolates sequenced with Oxford Nanopore  
690 have been deposited at NCBI (Table S1). We downloaded the Af293 reference assembly  
691 (accession: GCF\_000002655.1) as well as 252 assemblies and annotations from Barber et al.  
692 2021 from NCBI, and 256 assemblies and annotations from Lofgren et al. 2022 from the  
693 associated Zenodo repository<sup>57</sup>. We subsequently reformatted the contig and gene identifiers to  
694 include genome codes generated as part of this study (Table S2). All scripts (including raw data  
695 for figure generation), genomic data used for this study, and results from differential expression  
696 tests are available through the following Figshare repository DOI: 10.6084/m9.figshare.26049703.

## 697 Acknowledgements

698 We thank Jacob Steenwyk for insightful feedback on an earlier draft of this manuscript.

## 699 Funding

700 This work was supported by the Office of the Vice Chancellor for Research and Graduate  
701 Education at the University of Wisconsin-Madison with funding from the Wisconsin Alumni  
702 Research Foundation to EGT; by funding from start-up funds from the Department of Plant  
703 Pathology at the University of Wisconsin-Madison and from the European Union's Horizon 2020  
704 research and innovation programme under the Marie Skłodowska-Curie grant agreement to EGT  
705 (grant number 890630); by the Swedish Research Council Formas (grant number 2019-01227)  
706 and the Swedish Research Council VR (grant number 2021-04290) to AAV. JES, CP, and RAC  
707 are supported by funding from the National Institutes of Health (grant no. 2R01AI130128), to RAC.  
708 JES is a CIFAR Fellow in the program Fungal Kingdom: Threats and Opportunities. Analyses and  
709 data management at UC Riverside was performed on the High-Performance Computing Center  
710 at the University of California, Riverside, in the Institute of Integrative Genome Biology, supported  
711 by grants from NSF (DBI-2215705) and NIH (S10-OD016290).

712

## 713 References

- 714 1. WHO Fungal Priority Pathogens List to Guide Research, Development and Public Health  
715 Action. (2022).
- 716 2. Denning, D. W. Global incidence and mortality of severe fungal disease. *Lancet Infect. Dis.*  
717 S1473-3099(23)00692–8 (2024) doi:10.1016/S1473-3099(23)00692-8.
- 718 3. Latgé, J.-P. & Chamilos, G. *Aspergillus fumigatus* and Aspergillosis in 2019. *Clin. Microbiol.*  
719 *Rev.* **33**, 10.1128/cmr.00140-18 (2019).
- 720 4. Kowalski, C. H. *et al.* Heterogeneity among Isolates Reveals that Fitness in Low Oxygen  
721 Correlates with *Aspergillus fumigatus* Virulence. *mBio* **7**, e01515-16 (2016).
- 722 5. Colabardini, A. C. *et al.* Heterogeneity in the transcriptional response of the human  
723 pathogen *Aspergillus fumigatus* to the antifungal agent caspofungin. *Genetics* **220**, iyab183  
724 (2022).
- 725 6. Horta, M. A. C. *et al.* Examination of Genome-Wide Ortholog Variation in Clinical and  
726 Environmental Isolates of the Fungal Pathogen *Aspergillus fumigatus*. *mBio* **13**, e01519-22  
727 (2022).
- 728 7. Keller, N. P. Heterogeneity Confounds Establishment of “a” Model Microbial Strain. *mBio* **8**,  
729 10.1128/mbio.00135-17 (2017).
- 730 8. Steenwyk, J. L., Rokas, A. & Goldman, G. H. Know the enemy and know yourself:  
731 Addressing cryptic fungal pathogens of humans and beyond. *PLoS Pathog.* **19**, e1011704  
732 (2023).
- 733 9. Lofgren, L. A., Ross, B. S., Cramer, R. A. & Stajich, J. E. The pan-genome of *Aspergillus*  
734 *fumigatus* provides a high-resolution view of its population structure revealing high levels of  
735 lineage-specific diversity driven by recombination. *PLOS Biol.* **20**, e3001890 (2022).
- 736 10. Barber, A. E. *et al.* *Aspergillus fumigatus* pan-genome analysis identifies genetic variants  
737 associated with human infection. *Nat. Microbiol.* **6**, 1526–1536 (2021).
- 738 11. Rhodes, J. *et al.* Population genomics confirms acquisition of drug-resistant *Aspergillus*  
739 *fumigatus* infection by humans from the environment. *Nat. Microbiol.* **7**, 663–674 (2022).
- 740 12. Hall, J. P. J., Harrison, E. & Baltrus, D. A. Introduction: the secret lives of microbial mobile  
741 genetic elements. *Philos. Trans. R. Soc. B Biol. Sci.* **377**, 20200460 (2022).
- 742 13. Aubert, D., Naas, T., Héritier, C., Poirel, L. & Nordmann, P. Functional characterization of  
743 IS1999, an IS4 family element involved in mobilization and expression of beta-lactam  
744 resistance genes. *J. Bacteriol.* **188**, 6506–6514 (2006).
- 745 14. Krishnan, P. *et al.* Transposable element insertions shape gene regulation and melanin  
746 production in a fungal pathogen of wheat. *BMC Biol.* **16**, 78 (2018).
- 747 15. Hottes, A. K. *et al.* Bacterial Adaptation through Loss of Function. *PLOS Genet.* **9**,  
748 e1003617 (2013).
- 749 16. Weisberg, A. J. & Chang, J. H. Mobile Genetic Element Flexibility as an Underlying Principle  
750 to Bacterial Evolution. *Annu. Rev. Microbiol.* **77**, null (2023).
- 751 17. Baquero, F. From pieces to patterns: evolutionary engineering in bacterial pathogens. *Nat.*  
752 *Rev. Microbiol.* **2**, 510–518 (2004).
- 753 18. Benler, S. *et al.* Cargo Genes of Tn7-Like Transposons Comprise an Enormous Diversity of

- 754 Defense Systems, Mobile Genetic Elements, and Antibiotic Resistance Genes. *mBio* **12**,  
755 e02938-21 (2021).
- 756 19. Gluck-Thaler, E. *et al.* Giant Starship Elements Mobilize Accessory Genes in Fungal  
757 Genomes. *Mol. Biol. Evol.* **39**, msac109 (2022).
- 758 20. Urquhart, A. S., Vogan, A. A., Gardiner, D. M. & Idnurm, A. Starships are active eukaryotic  
759 transposable elements mobilized by a new family of tyrosine recombinases. *Proc. Natl.*  
760 *Acad. Sci. U. S. A.* **120**, e2214521120 (2023).
- 761 21. Gluck-Thaler, E. & Vogan, A. A. Systematic identification of cargo-mobilizing genetic  
762 elements reveals new dimensions of eukaryotic diversity. *Nucleic Acids Res.* gkae327  
763 (2024) doi:10.1093/nar/gkae327.
- 764 22. Gourlie, R. *et al.* The pangenome of the wheat pathogen *Pyrenophora tritici-repentis* reveals  
765 novel transposons associated with necrotrophic effectors ToxA and ToxB. *BMC Biol.* **20**,  
766 239 (2022).
- 767 23. Urquhart, A. S., Chong, N. F., Yang, Y. & Idnurm, A. A large transposable element mediates  
768 metal resistance in the fungus *Paecilomyces variotii*. *Curr. Biol.* **32**, 937-950.e5 (2022).
- 769 24. Urquhart, A. S., Gluck-Thaler, E. & Vogan, A. A. Gene acquisition by giant transposons  
770 primes eukaryotes for rapid evolution via horizontal gene transfer. 2023.11.22.568313  
771 Preprint at <https://doi.org/10.1101/2023.11.22.568313> (2023).
- 772 25. Bucknell, A. *et al.* Sanctuary: A Starship transposon facilitating the movement of the  
773 virulence factor ToxA in fungal wheat pathogens. 2024.03.04.583430 Preprint at  
774 <https://doi.org/10.1101/2024.03.04.583430> (2024).
- 775 26. Pain, A. *et al.* Insight into the genome of *Aspergillus fumigatus*: analysis of a 922 kb region  
776 encompassing the nitrate assimilation gene cluster. *Fungal Genet. Biol. FG B* **41**, 443–453  
777 (2004).
- 778 27. Monod, M. *et al.* Virulence of alkaline protease-deficient mutants of *Aspergillus fumigatus*.  
779 *FEMS Microbiol. Lett.* **106**, 39–46 (1993).
- 780 28. Kowalski, C. H., Morelli, K. A., Stajich, J. E., Nadell, C. D. & Cramer, R. A. A  
781 Heterogeneously Expressed Gene Family Modulates the Biofilm Architecture and Hypoxic  
782 Growth of *Aspergillus fumigatus*. *mBio* **12**, e03579-20 (2021).
- 783 29. Wicker, T. *et al.* A unified classification system for eukaryotic transposable elements. *Nat.*  
784 *Rev. Genet.* **8**, 973–982 (2007).
- 785 30. Lind, A. L. *et al.* Drivers of genetic diversity in secondary metabolic gene clusters within a  
786 fungal species. *PLoS Biol.* **15**, e2003583 (2017).
- 787 31. Abdolrasouli, A. *et al.* Genomic Context of Azole Resistance Mutations in *Aspergillus*  
788 *fumigatus* Determined Using Whole-Genome Sequencing. *mBio* **6**, e00536-15 (2015).
- 789 32. Ma, K. *et al.* Characterization and Biosynthesis of a Rare Fungal Hopane-Type Triterpenoid  
790 Glycoside Involved in the Antistress Property of *Aspergillus fumigatus*. *Org. Lett.* **21**, 3252–  
791 3256 (2019).
- 792 33. Brown, N. A. & Goldman, G. H. The contribution of *Aspergillus fumigatus* stress responses  
793 to virulence and antifungal resistance. *J. Microbiol.* **54**, 243–253 (2016).
- 794 34. Steenwyk, J. L. *et al.* Genomic and Phenotypic Analysis of COVID-19-Associated  
795 Pulmonary Aspergillosis Isolates of *Aspergillus fumigatus*. *Microbiol. Spectr.* **9**,

- 796 10.1128/spectrum.00010-21 (2021).
- 797 35. Raffa, N., Oshero, N. & Keller, N. P. Copper Utilization, Regulation, and Acquisition by  
798 *Aspergillus fumigatus*. *Int. J. Mol. Sci.* **20**, 1980 (2019).
- 799 36. Bignell, E., Cairns, T. C., Throckmorton, K., Nierman, W. C. & Keller, N. P. Secondary  
800 metabolite arsenal of an opportunistic pathogenic fungus. *Philos. Trans. R. Soc. B Biol. Sci.*  
801 **371**, 20160023 (2016).
- 802 37. Abad, A. *et al.* What makes *Aspergillus fumigatus* a successful pathogen? Genes and  
803 molecules involved in invasive aspergillosis. *Rev. Iberoam. Micol.* **27**, 155–182 (2010).
- 804 38. Auxier, B. *et al.* Identification of heterokaryon incompatibility genes in *Aspergillus fumigatus*  
805 highlights a narrow footprint of ancient balancing selection. 2022.11.25.517501 Preprint at  
806 <https://doi.org/10.1101/2022.11.25.517501> (2022).
- 807 39. Stroe, M. C. *et al.* Targeted induction of a silent fungal gene cluster encoding the bacteria-  
808 specific germination inhibitor fumigermin. *eLife* **9**, e52541 (2020).
- 809 40. Kowalski, C. H. *et al.* Fungal biofilm morphology impacts hypoxia fitness and disease  
810 progression. *Nat. Microbiol.* **4**, 2430–2441 (2019).
- 811 41. Rokas, A., Mead, M. E., Steeny, J. L., Oberlies, N. H. & Goldman, G. H. Evolving moldy  
812 murderers: *Aspergillus* section *Fumigati* as a model for studying the repeated evolution of  
813 fungal pathogenicity. *PLOS Pathog.* **16**, e1008315 (2020).
- 814 42. Shaw, L. P. *et al.* Niche and local geography shape the pangenome of wastewater- and  
815 livestock-associated *Enterobacteriaceae*. *Sci. Adv.* **7**, eabe3868 (2021).
- 816 43. Shimizu, K. & Keller, N. P. Genetic involvement of a cAMP-dependent protein kinase in a G  
817 protein signaling pathway regulating morphological and chemical transitions in *Aspergillus*  
818 *nidulans*. *Genetics* **157**, 591–600 (2001).
- 819 44. Carter-House, D., Stajich, J., Unruh, S. & Kurbessoian, T. Fungal CTAB DNA Extraction.  
820 (2020).
- 821 45. Koren, S. *et al.* Canu: scalable and accurate long-read assembly via adaptive k-mer  
822 weighting and repeat separation. *Genome Res.* **27**, 722–736 (2017).
- 823 46. Walker, B. J. *et al.* Pilon: an integrated tool for comprehensive microbial variant detection  
824 and genome assembly improvement. *PLoS One* **9**, e112963 (2014).
- 825 47. Palmer, J. M. & Stajich, J. E. Automatic assembly for the fungi (AAFTF): genome assembly  
826 pipeline. Zenodo <https://doi.org/10.5281/zenodo.7439973> (2022).
- 827 48. Manni, M., Berkeley, M. R., Seppey, M., Simão, F. A. & Zdobnov, E. M. BUSCO Update:  
828 Novel and Streamlined Workflows along with Broader and Deeper Phylogenetic Coverage  
829 for Scoring of Eukaryotic, Prokaryotic, and Viral Genomes. *Mol. Biol. Evol.* **38**, 4647–4654  
830 (2021).
- 831 49. Palmer, J. M. & Stajich, J. Funannotate v1.8.1: Eukaryotic genome annotation. Zenodo  
832 <https://doi.org/10.5281/zenodo.4054262> (2020).
- 833 50. Haas, B. J. *et al.* Improving the *Arabidopsis* genome annotation using maximal transcript  
834 alignment assemblies. *Nucleic Acids Res.* **31**, 5654–5666 (2003).
- 835 51. Jones, P. *et al.* InterProScan 5: genome-scale protein function classification. *Bioinformatics*  
836 **30**, 1236–1240 (2014).
- 837 52. Cantalapiedra, C. P., Hernández-Plaza, A., Letunic, I., Bork, P. & Huerta-Cepas, J.

- 838 eggNOG-mapper v2: Functional Annotation, Orthology Assignments, and Domain Prediction  
839 at the Metagenomic Scale. *Mol. Biol. Evol.* (2021) doi:10.1093/molbev/msab293.
- 840 53. Zheng, J. *et al.* dbCAN3: automated carbohydrate-active enzyme and substrate annotation.  
841 *Nucleic Acids Res.* **51**, W115–W121 (2023).
- 842 54. Blin, K. *et al.* antiSMASH 6.0: improving cluster detection and comparison capabilities.  
843 *Nucleic Acids Res.* **49**, W29–W35 (2021).
- 844 55. Nawrocki, E. P. & Eddy, S. R. Infernal 1.1: 100-fold faster RNA homology searches.  
845 *Bioinformatics* **29**, 2933–2935 (2013).
- 846 56. Purcell, S. *et al.* PLINK: A Tool Set for Whole-Genome Association and Population-Based  
847 Linkage Analyses. *Am. J. Hum. Genet.* **81**, 559–575 (2007).
- 848 57. Lofgren, L. A., Ross, B., Cramer Jr, R. A. & Stajich, J. E. Aspergillus fumigatus pangenome  
849 dataset. Zenodo <https://doi.org/10.5281/zenodo.5775266> (2021).
- 850 58. Emms, D. M. & Kelly, S. OrthoFinder: solving fundamental biases in whole genome  
851 comparisons dramatically improves orthogroup inference accuracy. *Genome Biol.* **16**, 157  
852 (2015).
- 853 59. Camacho, C. *et al.* BLAST+: architecture and applications. *BMC Bioinformatics* **10**, 421  
854 (2009).
- 855 60. Marçais, G. *et al.* MUMmer4: A fast and versatile genome alignment system. *PLOS Comput.*  
856 *Biol.* **14**, e1005944 (2018).
- 857 61. Nattestad, M., Aboukhalil, R., Chin, C.-S. & Schatz, M. C. Ribbon: intuitive visualization for  
858 complex genomic variation. *Bioinformatics* **37**, 413–415 (2020).
- 859 62. Bowyer, P., Currin, A., Delneri, D. & Fraczek, M. G. Telomere-to-telomere genome  
860 sequence of the model mould pathogen *Aspergillus fumigatus*. *Nat. Commun.* **13**, 5394  
861 (2022).
- 862 63. Li, H. Minimap2: pairwise alignment for nucleotide sequences. *Bioinformatics* **34**, 3094–  
863 3100 (2018).
- 864 64. Thorvaldsdóttir, H., Robinson, J. T. & Mesirov, J. P. Integrative Genomics Viewer (IGV):  
865 high-performance genomics data visualization and exploration. *Brief. Bioinform.* **14**, 178–  
866 192 (2013).
- 867 65. Levy Karin, E., Mirdita, M. & Söding, J. MetaEuk—sensitive, high-throughput gene  
868 discovery, and annotation for large-scale eukaryotic metagenomics. *Microbiome* **8**, 48  
869 (2020).
- 870 66. Ayad, L. A. K., Pissis, S. P. & Polychronopoulos, D. CNEFinder: finding conserved non-  
871 coding elements in genomes. *Bioinforma. Oxf. Engl.* **34**, i743–i747 (2018).
- 872 67. Katoh, K. & Standley, D. M. MAFFT Multiple Sequence Alignment Software Version 7:  
873 Improvements in Performance and Usability. *Mol. Biol. Evol.* **30**, 772–780 (2013).
- 874 68. Hauser, M., Steinegger, M. & Söding, J. MMseqs software suite for fast and deep clustering  
875 and searching of large protein sequence sets. *Bioinformatics* **32**, 1323–1330 (2016).
- 876 69. Brown, C. T. & Irber, L. sourmash: a library for MinHash sketching of DNA. *J. Open Source*  
877 *Softw.* **1**, 27 (2016).
- 878 70. Enright, A. J., Van Dongen, S. & Ouzounis, C. A. An efficient algorithm for large-scale  
879 detection of protein families. *Nucleic Acids Res.* **30**, 1575–1584 (2002).

- 880 71. Sahlin, K. Strobealign: flexible seed size enables ultra-fast and accurate read alignment.  
881 *Genome Biol.* **23**, 260 (2022).
- 882 72. Patro, R., Duggal, G., Love, M. I., Irizarry, R. A. & Kingsford, C. Salmon provides fast and  
883 bias-aware quantification of transcript expression. *Nat. Methods* **14**, 417–419 (2017).
- 884 73. Dobin, A. *et al.* STAR: ultrafast universal RNA-seq aligner. *Bioinformatics* **29**, 15–21 (2013).
- 885 74. Rezaie, N., Reese, F. & Mortazavi, A. PyWGCNA: a Python package for weighted gene co-  
886 expression network analysis. *Bioinformatics* **39**, btad415 (2023).
- 887 75. Love, M. I., Huber, W. & Anders, S. Moderated estimation of fold change and dispersion for  
888 RNA-seq data with DESeq2. *Genome Biol.* **15**, 550 (2014).
- 889 76. MetaVolcanoR. *Bioconductor* <http://bioconductor.org/packages/MetaVolcanoR/>.
- 890 77. Virtanen, P. *et al.* SciPy 1.0: fundamental algorithms for scientific computing in Python. *Nat.*  
891 *Methods* **17**, 261–272 (2020).
- 892 78. Kolberg, L., Raudvere, U., Kuzmin, I., Vilo, J. & Peterson, H. gprofiler2 -- an R package for  
893 gene list functional enrichment analysis and namespace conversion toolset g:Profiler.  
894 *F1000Research* **9**, ELIXIR-709 (2020).
- 895 79. Krzywinski, M. I. *et al.* Circos: An information aesthetic for comparative genomics. *Genome*  
896 *Res.* (2009) doi:10.1101/gr.092759.109.
- 897 80. Hackl T, Ankenbrand M, & van Adrichem B. gggenomes: A Grammar of Graphics for  
898 Comparative Genomics. (2023).
- 899 81. Wickham, H. *Ggplot2: Elegant Graphics for Data Analysis*. (Springer International  
900 Publishing, Cham, 2016). doi:10.1007/978-3-319-24277-4.
- 901 82. Filho, A. P. da C. *et al.* Aspergillus fumigatus G-Protein Coupled Receptors GprM and GprJ  
902 Are Important for the Regulation of the Cell Wall Integrity Pathway, Secondary Metabolite  
903 Production, and Virulence. *mBio* **11**, 10.1128/mbio.02458-20 (2020).
- 904

## 905 Supplemental information and results

### 906 *Starship* frequencies

907 The population-level frequency of high-confidence *Starships* ranges from 1-60%, with 13 of the  
908 high-confidence *Starships* present in <10% of strains and no *Starship* present in more than 60%  
909 of strains (Table S6). Each high-confidence *Starship* is present across multiple individuals;  
910 however, any given *Starship* element is only present at most once in a genome, with only 3  
911 exceptions that likely involve recently degraded copies, suggesting some mechanism for  
912 controlling their copy number (e.g., repeat-induced point mutation<sup>20</sup>). Individual elements typically  
913 segregate at low frequencies, with each segregating site containing on average an inserted  
914 element in just 0.4% of strains across the 20 high-confidence *Starships* (range = 0.2-52.3%, std.  
915 dev. = 6.5%, n = 154; Fig. 3B). However, multiple insertion sites often exist for a given element  
916 such that each high-confidence *Starship* is present on average in 4.35 different regions (range =  
917 1-15, std. dev. = 3.92).

### 918 Differential expression of *Starship* captains and cargo

919 Patterns of transcript coverage, transcript abundance, and differential expression of *Starship*-  
920 associated genes were generally heterogeneous, with various strain-, treatment- and strain by  
921 treatment interactions. The transcriptional profile for many *Starships* is patchy, and not all  
922 *Starship*-mobilized genes are expressed in response to experimental conditions. Only certain  
923 cargo genes have the minimum required evidence for constitutive expression: a median transcript  
924 coverage of 1 across the gene body. A greater number of genes present in *Starships* from *A.*  
925 *fumigatus* Af293 (Fig. S12A) have core gene transcript coverage greater than this threshold,  
926 compared to genes in A1163 (Fig. S12C) and CEA10 (Fig. S12B) *Starships*. Interestingly, specific  
927 studies of Af293 or CEA10 which tested exposure to heatshock (PRJDB6203), hypoxia  
928 (PRJNA144647), *in vitro* infections (PRJEB1583, PRJNA399754, PRJNA399754). and various  
929 gene knock-out experiments (PRJNA390719, PRJNA396210, and PRJNA601094) have  
930 consistently reported expression of all genes across the *Starship* element.

931  
932 Captain genes of multiple *Starships* from Af293 and CEA10 had decreased transcript abundance  
933 associated with “infection” studies. Samples of a study performing an experimental infection using  
934 a murine model (PRJNA421149) had near-zero transcript abundances of captain genes from  
935 Af293 *Starships* *Janus h2*, *Osiris h3*, and *Gnosis h1*. However, this was not found within samples  
936 of a different study of an Af293 infection of human pneumocyte cell lines (PRJNA399754). Near-  
937 zero abundances were also found for a different set of captain genes, within CEA10 *Starships*  
938 *Tardis h1*, *Logos h2*, and *Gnosis h3*, from an *in vitro* infection study using human cell lines (Fig.  
939 S11), suggesting that the transcriptional response of *Starship* captains within the infection  
940 environment differs between strains.

941

942 Specific treatments applied within a single study can have a contrasting influence on the prevailing  
943 expression patterns of captain genes. Expression of the *Tardis h1* captain gene in Af293 is  
944 generally decreased across nutrient supplementation studies compared to controls (Fig. 5B). Yet,  
945 supplementation of glucose and xylose has a positive and negative influence on captain  
946 expression, respectively, compared to controls with nutrient media<sup>82</sup>. Similarly, expression of  
947 CEA10 *Logos h1* and *h2* captain genes both decreased and increased, with supplementation of  
948 acetate (PRJNA668271), respectively, compared to nutrient media controls containing dilute  
949 acetate (0.1%) (Fig. 5D). Together, these gene expression datasets demonstrate the context-  
950 dependent expression of captain genes, which we speculate would lead to variation in *Starship*  
951 transposition rates across different environments and strain backgrounds.

952  
953 Similar to captain genes, the expression patterns of cargo genes within *Starships* are  
954 heterogeneous. The transcriptional profile of *Starships* is punctuated with expression of cargo  
955 genes (Figure SH), which can have substantial transcript coverage even in the absence of captain  
956 expression, suggesting that the transcriptional regulation of these cargo genes are decoupled  
957 from transposition. Of particular note are the genes that form biosynthetic gene clusters (BGC)  
958 which reside within *Starships*. In Af293, 47 BGC genes across six *Starships* (*Gnosis h1*, *Lamia*  
959 *h4*, *Nebuchadnezzar h1*, *Nebuchadnezzar h2*, *Osiris h4*, *Tardis h1*) are DE in one or more of the  
960 treatment categories investigated in this study. At least one gene from the BGCs across these six  
961 *Starships* are DE in response to caspofungin exposure, from a specific Af293 study  
962 (PRJNA472460). Furthermore, multiple genes associated with a BGC present in *Osiris h4*  
963 (AFUA\_3G02580, AFUA\_3G02600, AFUA\_3G02620, AFUA\_3G02630, AFUA\_3G02640) have  
964 significantly increased expression compared to controls. Interestingly, generally fewer genes in  
965 BGCs are DE in Af293 “antifungal” or “nutrient” studies. Relatively fewer *Starship* BGC genes are  
966 DE in other strains. Notably, a collection of cargo genes from Fumihopaside A and terpene  
967 biosynthesis (CEA10-lr\_006118) BGCs in CEA10 *Gnosis h2* have decreased expression during  
968 an *in vitro* infection of a human cell line. Cargo genes within *Osiris h4* that increased expression  
969 under both antifungal exposure and nutrient manipulation included multiple genes from the  
970 putative NR-PKS BGC (Fig. S13).

971  
972 As a human pathogen, we were also interested in *A. fumigatus* genes that have specific relevance  
973 to virulence, such as genes within *hrmA*-associated cluster (HAC). Two HAC genes present in  
974 *Nebuchadnezzar h1*, *cgnA* and *bafA*, have near-zero transcript abundances within samples from  
975 an Af293 study of an experimental infection of a murine model (PRJNA421149). However, genes  
976 within the HAC cluster were only DE within certain nutrient and antifungal studies. Specifically,  
977 *cgnA* (AFUA\_5G14910) and *hrmA* (AFUA\_5G14900) both have increased expression within  
978 Af293 samples supplemented with calcium, and *bafA* (AFUA\_3G04070) has decreased  
979 expression in CEA10 samples under caspofungin exposure (Fig. 5A).

980  
981 Multiple DE cargo genes serve putative functions that are relevant for the metabolic or enzymatic  
982 activity of the cell. Collections of cargo genes within the Af293 *Starships* *Lamia h4* and *Osiris h4*  
983 have consistently increased expression from studies employing nutrient manipulation treatments

984 compared to controls (Fig. S13). This includes several genes in *Lamia h4* with a putative role in  
985 enzymatic secretion (e.g., glycosyl hydrolases, phosphotransferases, and dehydrogenases).  
986 Genes with domains relevant to dehydrogenases (NAD binding domains) were generally positive  
987 DEGs within antifungal and nutrient studies of Af293 and A1163, respectively.

988  
989 Genes with a putative role in specific molecular functions were also consistently DE in *Starships*.  
990 We found that genes involved in zinc ion binding activity (IBR) (negative DEG in Af293 antifungal  
991 and positive DEG in CEA10 antifungal), dynamin-like GTPase domain and BTB (both highly  
992 negative DEGS in CEA10 *Logos h1* within infection studies). In Af293 *Tardis h1*, a gene with a  
993 putative role in structural molecular activity (domains for Cytochrome b5-like Heme/Steroid  
994 binding and flocculin; AFUA\_8G06250) has increased expression in nutrient supplementation.  
995 Whereas HATPase\_c/HisKA response regulator (AFUA\_8G06140) and glycoside  
996 hydrolase/lipase (AFUA\_8G06350) have decreased expression in nutrient supplementation in the  
997 same *Starship*.

998  
999 Additional cargo genes of interest may convey resistance to environmental stressors. Two genes  
1000 involved in arsenic detoxification, present within *Nebuchadnezzar h1*, were found to be DE in  
1001 Af293 and CEA10 studies. Arsenate reductase (AFUA\_5G15000) in *Nebuchadnezzar h1* was  
1002 found to both have increased and decreased expression within the CEA10 and Af293 copies,  
1003 respectively. Three additional genes within this pathway were found to be DE in response across  
1004 “antifungal” or “infection” studies (Fig. 5B). Two of these genes in in Af293 *Nebuchadnezzar h1*,  
1005 arsenate methyl-transferase (AFUA\_5G15020) and arsenite efflux transporter (AFUA\_5G15010),  
1006 were found to have either increased or decreased expression levels under caspofungin exposure,  
1007 respectively. The third, arsenite permease (AFUA\_1G16100) has decreased expression in Af293  
1008 infection studies.

## 1009 *Starship* co-expression networks

1010 We performed weighted gene co-expression network analysis (WGCNA) using *PyWGCNA* to  
1011 construct gene co-expression networks for each of the three *A. fumigatus* reference strains Af293,  
1012 CEA10, and A1163. Overall, we found that genes within or between *Starships* are more strongly  
1013 co-expressed together than with non-*Starship* genes, based on pairwise comparisons of the  
1014 distribution of scores in the topological overlap matrices (TOM) (corrected p-values < 0.01 for all  
1015 comparisons; Fig. S14). This suggests that a tighter transcriptional relationship exists between  
1016 genes mobilized by *Starships* compared to co-expression with other genes in the genome.

1017  
1018 Genes in the *A. fumigatus* Af293 co-expression network were resolved into 27 modules (Table  
1019 S24). The majority of genes found within each module are not contained within a *Starship*, yet  
1020 almost all modules contain one or more *Starship* genes, including those previously identified as  
1021 DEGs (Table S24). Modules were selected for further analyses based on the correlation of their  
1022 gene expression profiles (WGCNA eigengenes) and their association with a treatment category  
1023 (“antifungal”, “infection”, or “nutrient”) or specific study (Fig. 5E & Fig. S15).

1024  
1025 To investigate functional compartmentalization of WGCNA modules, we performed enrichment  
1026 tests and identified which GO/KEGG terms are significantly overrepresented within each module.  
1027 Genes in module “2” are significantly enriched in functions including the production of  
1028 antimicrobial secondary metabolites (fumagillin), the secretion of *A. fumigatus* mycotoxins  
1029 (helvolic acid), proteins for heme binding, and synthesis of immunosuppressive compounds  
1030 (endocrain) (Table S25SV).

1031  
1032 To identify which genes are most strongly co-expressed with *Starship* cargo or captain genes, we  
1033 subsetted the co-expression network to keep only the top 10 edges that were made between any  
1034 pair of genes or any gene and a *Starship* captain. Two modules within the Af293 co-expression  
1035 network (“2” and “15”) are significantly more commonly co-expressed within samples from a single  
1036 infection study of Af293 (PRJEB1583; Fig. 5E). The connections with the highest TOM scores in  
1037 module “2” include those between an IBR finger domain protein within the *Starship* Lamia h4  
1038 (AFUA\_1G00150) and genes involved in RNA binding pathways (AFUA\_6G12070), as well as  
1039 genes for alpha-amylase (AFUA\_2G03230) and anthrone oxygenase (AFUA\_4G00225) (Fig.  
1040 5D). Genes within the module “15” include those tightly connected to the expression of F-box  
1041 domain protein within *Lamia h4*. Genes within module “15” are enriched in glycerophospholipid  
1042 metabolism (Table S25SV). These co-expression relationships provide insight into how *Starships*-  
1043 mobilized genes integrate into the existing transcriptional network in *A. fumigatus* strains.

1044  
1045 Module “3” is significantly associated with increased expression within a single study of an  
1046 experimental infection in mice (PRJNA693756) (Fig. 5E & S15). Genes within module “3” are  
1047 enriched for genes in ribosome biogenesis in eukaryotes, carbon metabolism, and pyruvate  
1048 metabolism (Table S25SV). The connections with the highest TOM scores in module “3”, include  
1049 genes co-expressed with Gnosis h1 captain gene: genes with predicted catalytic activity  
1050 (AFUA\_1G12370), zinc-containing alcohol dehydrogenase (AFUA\_2G00970), mitochondrial  
1051 respiration (AFUA\_2G06020), and exonuclease activity/DNA-directed DNA polymerase  
1052 activity/role in mitochondrial DNA replication and mitochondrion localization (AFUA\_5G12640).

1053  
1054 Module “7” is significantly associated with two studies testing supplementation with 5,8-  
1055 dihydroxyoctadecadienoic acid (PRJNA658306) and lipo-chitooligosaccharides (PRJNA642658)  
1056 in Af293 (Fig. 5E & S15). The focus of both of these studies is to understand how these  
1057 supplementations impact the regulation of fungal growth and development. The connections with  
1058 the highest TOM scores in the module “7”, include genes co-expressed with captain genes of  
1059 Tardis h1 and Osiris h3. Osiris h3 captain co-expressed with predicted RNA binding, ribonuclease  
1060 III activity and role in RNA processing (AFUA\_3G03050). The connections made in this module  
1061 with *Starship* genes present themselves as good candidates for future research to understand  
1062 which genes are expressed along with transposition.

## 1063 Figure legends

1064 Figure 1: At least 20 distinct *Starships* carrying hundreds of protein-coding genes vary in their  
1065 presence/absence across *Aspergillus fumigatus* strains. A) Top: a SNP-based maximum  
1066 likelihood tree of 220 *A. fumigatus* strains, color-coded according to phylogenetic clade (sensu  
1067 Lofgren et al., 2022)<sup>9</sup>. Bottom: A heatmap depicting the presence (gray) and absence (white) of  
1068 20 high-confidence *Starships* in each isolate. B) Schematics and sequence alignments of the type  
1069 elements from 20 high-confidence *Starships*, where links between schematics represent alignable  
1070 regions  $\geq 500\text{bp}$  and  $\geq 80\%$  nucleotide sequence identity and arrows represent predicted coding  
1071 sequences. C) A donut chart summarizing the number of distinct types of *Starships* by the quality  
1072 of their prediction. D) A Venn diagram indicating the number of shared and unique high-  
1073 confidence *Starships* in the reference strains Af293 and CEA10 (Table S7). E) A scatterplot  
1074 depicting pairwise comparisons of SNP-based Identity by State (IBS) and Jaccard similarity in  
1075 high-confidence *Starship* presence/absence profiles between 150 Clade 1 strains (Table S8).

1076  
1077 Figure 2: *Starships* are enriched in accessory genes whose presence/absence and genomic  
1078 location vary across *Aspergillus fumigatus* strains. All panels visualize data derived from 13  
1079 reference-quality *A. fumigatus* assemblies and the 20 high-confidence *Starships* ( $n = 459$   
1080 elements total). A) Box-and-whisker plots summarizing the total percentage of nucleotide  
1081 sequence and predicted genes carried by *Starships* per genome. B) Donut charts summarizing  
1082 the percentages of gene orthogroups in the core, accessory, singleton, and *Starship*-associated  
1083 compartments of the *A. fumigatus* pangenome (Table S10). C) Iceberg plots summarizing the  
1084 genomic locations of the single best BLASTp hits ( $\geq 90\%$  identity,  $\geq 33\%$  query coverage) to the  
1085 cargo genes from the type elements of all 20 high-confidence *Starships* (left) and two individual  
1086 *Starships* (right; Table S12). Each column in the iceberg plot represents a cargo gene and is  
1087 color-coded according to the genomic location of hits (full dataset in Fig. S4).

1088  
1089 Figure 3: *Starships* and their insertion sites are distributed across all major chromosomes in the  
1090 *Aspergillus fumigatus* genome. A) A Circos plot summarizing all inserted *Starships* (in red) and  
1091 all genomic regions containing either an empty insertion site or a fragmented *Starship* (in black,  
1092 along perimeter and labeled with the *r* prefix) in the 8 chromosomes of the *A. fumigatus* reference  
1093 strain Af293 (Table S14). All genomic regions contain a *Starship* insertion in some other individual  
1094 from the 519 strain population. B) Barcharts summarizing the genotypes of segregating genomic  
1095 regions associated with the four most active high-confidence elements in the *A. fumigatus* 519  
1096 strain population (Table S16; full dataset in Fig. S6). If an isolate did not have any *Starships* within  
1097 a given region, it was assigned either an “empty” or “fragmented” genotype (Methods). C) A  
1098 scatterplot summarizing the relationship between the number of genomic regions containing a  
1099 given *Starship* and the total number of copies of that *Starship* in the 519 *A. fumigatus* strain  
1100 population, where each point represents one of the 20 high-confidence *Starships*. A line derived

1101 from a linear regression model is superimposed, with shaded 95% confidence intervals drawn in  
1102 gray.

1103

1104 Figure 4: *Starships* mobilize adaptive traits and generate allelic diversity among *Aspergillus*  
1105 *fumigatus* strains. Schematics and alignments of: A) *Starship Lamia h2* and *h4*, which carry the  
1106 biosynthetic gene cluster (BGC) encoding the polyketide secondary metabolite Fumigermin<sup>39</sup>,  
1107 shown inserted at 3 independent sites. B) *Starship Gnosis h2* carrying the BGC encoding the  
1108 terpene secondary metabolite Fumihopaside A<sup>32</sup>, shown inserted at 2 independent sites. C) a  
1109 large region on Chromosome 3 previously identified as an idiomorphic BGC<sup>30</sup> containing multiple  
1110 segregating *Starship* insertions and various combinations of putative BGCs, including a a non-  
1111 reducing polyketide synthase (NR-PKS) BGC carried by *Starship Osiris h4*. *Starships* from the  
1112 *Osiris navis* specifically insert in 5S rDNA sequence and are predicted to fragment it (annotated  
1113 by two vertical gray bars). D) Eight *Starships* in the reference strains Af293 and CEA10 that all  
1114 carry homologs of *biofilm architecture factor A (bafA)*<sup>28</sup>. *Starship Nebuchadnezzar h1 (Neb. h1)*  
1115 carries *bafA* as part of the H<sub>A</sub>AC (*hrmA*-associated gene cluster), while *Starship navis10-var35*  
1116 carries *bafB* as part of H<sub>B</sub>AC and *Starship Osiris h3* carries *bafC* as part of H<sub>C</sub>AC<sup>28</sup>. Only a portion  
1117 of *Starship Lamia h4* is visualized for figure legibility. All data for A-D was collected from the 519  
1118 *A. fumigatus* strain population (Table S5). Links between schematics represent alignable regions  
1119  $\geq 5000$ bp and  $\geq 95\%$  nucleotide sequence identity and arrows represent predicted coding  
1120 sequences. Abbreviations: polyketide synthase (PKS); non-ribosomal peptide synthetase  
1121 (NRPS); highly reducing (HR).

1122

1123 Figure 5: A) A heatmap of transcript abundances ( $\log_{10}$ TPM) of *Starship* captain tyrosine  
1124 recombinase genes (top) and genes within the *hrmA*-associated cluster (HAC; bottom), collapsed  
1125 across treatment replicates, for 11 RNAseq studies from *A. fumigatus* Af293. B) Results from  
1126 differential expression (DE) tests for select *Starships*, treatment categories, and strain  
1127 combinations. Only genes with valid output from DE tests are shown, and only genes with  
1128 significantly DE are labeled with gene codes. Genes with extreme count outliers, as determined  
1129 by Cook's Distance in DESeq2, do not have valid p-values and are labeled with an asterisk (“\*”).  
1130 DE based on a single study are shown as  $\log_2$  fold-change ( $\log_2$ FC) in black with standard error  
1131 bars, whereas DE genes identified across multiple studies are represented with summarized  
1132  $\log_2$ FC values from a random effects model (REM) and coloured by “sign-consistency”, the  
1133 number of studies that reported DE in the positive (+1) or negative (-1) direction, centered around  
1134 0. Labels in bold font represent DEGs that are significantly DE in more than one study. C) The  
1135 results of a weighted gene co-expression network analysis (WGCNA) constructed from 14  
1136 “antifungal”, “infection”, and “nutrient” RNAseq studies represented using UMAP clustering based  
1137 on the co-expression eigengene values for all genes in the *A. fumigatus* Af293 genome. Non-  
1138 *Starship* genes present within modules of interest are shown in blue, while all *Starship* genes are  
1139 shown in red, with those genes within modules of interest having a black outline. D) Genes within  
1140 modules that were significantly associated with samples from specific treatment categories or

1141 studies were used to construct sub-networks which contained the top 10 edges in the network  
1142 that were made between any pair of genes or any gene and a *Starship* captain. The connections  
1143 between genes (edges) are based on the topological overlap matrix (TOM) for each module, and  
1144 have been 0-1 scaled. E) Boxplots of eigengene values from WGCNA, akin to a weighted average  
1145 expression profile, indicate the extent of co-expression (correlation) of the genes present within  
1146 each module. Pairwise comparisons of module eigengene values determined if a module was  
1147 significantly associated with samples from specific treatment categories or studies (Fig. S15).

## 1148 Supplemental figure legends

1149 Figure S1: Counts of starfish-predicted *Starships* per *Aspergillus fumigatus* strain (n = 519),  
1150 broken up by assembly project (either the 12 Oxford Nanopore Assemblies generated by study  
1151 plus the AF293 reference genome, or from Lofgren et al 2022 or Barber et al 2021; Table S2). A)  
1152 Counts of *Starships* with either 'insert' or 'flank' boundaries, which are derived directly from  
1153 pairwise genome alignments against a putative insertion site. B) Counts of *Starships* with 'insert'  
1154 or 'flank' boundaries plus those with 'extend' boundaries, which are derived from aligning genomic  
1155 sequences to known *Starship* sequences. Insert and flank boundaries are associated with full-  
1156 length *Starship* elements, while extend boundaries may be associated with either full-length  
1157 *Starship* elements or element fragments.

1158  
1159 Figure S2: Pairwise genome alignments of the CEA10 isolate sequenced by this study and the  
1160 CEA10 isolate from BioSample SAMN28487501 demonstrating *Starship* movement.  
1161 *Nebuchadnezzar h1* is present on Chromosome 6 in the SAMN28487501 isolate and absent at  
1162 the corresponding locus in this study's sequenced isolate. Conversely, *Nebuchadnezzar h1* is  
1163 present on Chromosome 4 in this study's isolate but absent from the corresponding locus in the  
1164 SAMN28487501 isolate.

1165 Figure S3: Screenshots from the IGV genome browser showing deletions and/or movement of  
1166 *Nebuchadnezzar h1* among different isolates of the same named strain sequenced by different  
1167 research groups (regions depicted in red denote *Nebuchadnezzar h1*). A. Nanopore long-read  
1168 sequences of strain CEA10-lr (generated in this study) mapped to the publicly available assembly  
1169 of a different isolate of this same strain (accession: SAMN28487501; sequenced by a different  
1170 research group). A zoom in of the genomic location of *Nebuchadnezzar h1* in the public genome  
1171 is shown (contig accession: CP097568.1). Only a single long-read supports the presence of the  
1172 *Starship* at this locus. All other reads indicate either a deletion (above) or presence elsewhere in  
1173 the genome (below). B. Illumina short-reads of strain ATCC46645 sequenced by a different  
1174 research group (accession: SRR7418935) mapped to the ATCC46645-lr genome sequenced in  
1175 this study. A zoom in of the genomic location of *Nebuchadnezzar h1* in ATCC46645-lr is shown  
1176 (contig accession: scaffold\_15). Three short-read tracks indicate a deletion of the *Starship*  
1177 (above). Note that more short reads are mapped than shown in the image. Track and color  
1178 descriptions can be found in the IGV manual.

1179

1180 Figure S4: Donut charts summarizing the percentages of gene orthogroups in the core,  
1181 accessory, singleton, and *Starship*-associated compartments of the *Aspergillus fumigatus*  
1182 pangenome, derived from the 13 reference-quality *A. fumigatus* strains and the expanded set of  
1183 54 high and medium-confidence *Starships* (n = 1818 elements total; Table S11).

1184

1185 Figure S5: Iceberg plots summarizing the genomic locations of the single best BLASTp hits ( $\geq 90\%$   
1186 identity,  $\geq 33\%$  query coverage) to the cargo genes from the type elements of the 20 high-  
1187 confidence *Starships* in 519 *Aspergillus fumigatus* assemblies (Table S13). Each column  
1188 represents a cargo gene. A) Results broken down by *Starship*, with columns arranged according  
1189 to gene order within each *Starship*. B) Compiled results across all 20 *Starships*, with columns  
1190 arranged according to the number of strains with BLASTp hits. Bars are colored according to the  
1191 genomic location in which the BLASTp hits are found.

1192

1193 Figure S6: Barcharts summarizing the genotypes of segregating genomic regions associated with  
1194 the 20 high-confidence elements in the *Aspergillus fumigatus* 519 strain population (Table S16).  
1195 If an isolate did not have any *Starships* within a given region, it was assigned either an “empty”  
1196 or “fragmented” genotype (Methods).

1197 Figure S7: The putative target site of *Starship Tardis* (indicated with an arrow) occurs more often  
1198 than you would expect by chance in the *Aspergillus fumigatus* genome. We estimated the copy  
1199 numbers of all k-mers of length 10 in the Af293 reference genome and found that the k-mer of  
1200 length 10 that corresponds to the putative target site of *Tardis* is present in high copy numbers  
1201 that exceed the expected genome-wide frequency of k-mers of this length ( $>99.99\%$ th percentile).

1202

1203 Figure S8: *Starships* mobilize genes encoding diverse metabolic functions. Barcharts  
1204 summarizing the presence of genes with metabolism-related COG (Clusters of Orthologous  
1205 Groups) annotations in the 20 high-confidence *Starships* in the 519 *Aspergillus fumigatus* strain  
1206 population (Table S18). The X-axis measures the percentage of copies of a given *Starship* that  
1207 carry at least 1 gene with an annotation of interest.

1208

1209 Figure S9: The Biofilm Architecture Factor (*baf*) gene family is closely associated with diverse  
1210 *Starships* in *Aspergillus fumigatus*. A maximum likelihood tree of *baf* sequences from the 519  
1211 *Aspergillus fumigatus* strain population. Branches with  $\geq 80\%$  SH-ALRT and  $\geq 95\%$  ultrafast  
1212 bootstrap support are in bold. *Baf* sequences found in *Starships* have the corresponding *Starship*  
1213 identification number appended to their right (Table S5). Sequences are color-coded according  
1214 to 6 corresponding *baf* clades of interest, and a summary of all the *Starship* types found  
1215 associated with each clade is printed on the right.

1216

1217 Figure S10: *Starships* are enriched in environmental and clinical strains. Barcharts summarizing  
1218 the proportion of strains from 475/479 *Aspergillus fumigatus* genotyped strains with known  
1219 isolation sources that have the 20 high-confidence *Starships*, broken up by isolation source.  
1220 Fisher's exact test P values for *Starship* enrichment across isolation source categories are shown  
1221 above each bar (adjusted for multiple comparisons using the Benjamini Hochberg procedure;  
1222 Table S20).

1223  
1224 Figure S11: A heatmap of transcript abundances ( $\log_{10}$  TPM) of *Starship* captain genes, collapsed  
1225 across treatment replicates, for RNAseq studies from *A. fumigatus* A1163 (A) and CEA10 (B).

1226 Figure S12: Heatmap of binary core transcript coverage across genes in *Starships* in strains  
1227 Af293 (A), CEA10 (B) and A1163 (C). Genes that have a median core transcript coverage greater  
1228 than 1 are shown here in blue, and values below 1 are shown in red.

1229  
1230 Figure S13: Differentially expressed *Starship*-mobilized genes (DEGs) displayed in volcano plots  
1231 across combinations of *A. fumigatus* strains and treatment categories. Differential expression  
1232 based on singleton studies are shown as  $\log_2$  fold-change ( $\log_2$ FC) in black with standard error  
1233 bars, whereas DEGs identified across multiple studies are represented with summarized  $\log_2$ FC  
1234 values from a random effects model (REM) and coloured by values "sign-consistency", the  
1235 number of studies that reported differential gene expression in the positive (+1) or negative (-1)  
1236 direction, centered around 0.

1237  
1238 Figure S14: Distributions of TOM scores from the WGCNA constructed from Af293 *A. fumigatus*  
1239 studies. TOM scores were separated into distinct categories for edges that connected any two  
1240 genes within a *Starships*, between different *Starships*, between *Starships* and the rest of the  
1241 genome, or between any two non-*Starship* genes in the genome were compared. These  
1242 distributions were compared using a Wilcoxon test ( $p > 0.05 = \text{"ns"}; p < 0.05 = \text{" "}, p < 0.01 = \text{"**"}; p < 0.001 = \text{"***"}; p < 0.0001 = \text{"****"}).$

1243  
1244  
1245 Figure S15: Heatmap displaying the correlation values for eigengenes in each module and their  
1246 association with samples from a specific study (labeled with BioProject IDs), or different levels of  
1247 experimental treatment category across studies. Cells of the heatmap are coloured by the  
1248 correlation value, as well as labeled in each cell. P-values from a pairwise comparison between  
1249 observations (*pdist*) are shown in parentheses.

## 1250 Supplemental table legends

1251  
1252 Table S1: Genome assembly statistics for the 12 strains sequenced with Oxford Nanopore long-  
1253 read technology

1254  
1255 Table S2: Metadata for publically available *Aspergillus fumigatus* strains  
1256

1257	Table S3: Manual annotation data of 86 Starship elements
1258	
1259	Table S4: Metadata for all starfish-predicted Starships
1260	
1261	Table S5: Sequence features of all starfish-predicted Starships in the 519 strain population
1262	
1263	Table S6: Frequencies of the 20 high-confidence Starships in the 519 strain population using the
1264	expanded dataset
1265	
1266	Table S7: Manual annotation of Starship elements in three <i>Aspergillus fumigatus</i> reference strains
1267	
1268	Table S8: Pairwise comparisons between strains of SNP identity by state and Starship repertoire
1269	similarity
1270	
1271	Table S9: Comparison of Starship coordinates with structural variants identified by Colabardini et
1272	al 2022 (doi: 10.1371/journal.pgen.1010001)
1273	
1274	Table S10: Orthogroup frequencies in the 519 strain population
1275	
1276	Table S11: Orthogroup frequencies in the 13 reference-quality strains
1277	
1278	Table S12: BLAST recovery of Starship cargo genes from the 13 reference-quality strains
1279	
1280	Table S13: BLAST recovery of Starship cargo genes from the 519 strain population
1281	
1282	Table S14: Genotyping of genomic regions with segregating Starship insertions
1283	
1284	Table S15: Starships in genotyped genomic regions with segregating Starship insertions
1285	
1286	Table S16: Summary of genotyping data for genomic regions with segregating Starship insertions
1287	
1288	Table S17: Coordinates of predicted 5s rDNA sequences in the 519 strain population
1289	
1290	Table S18: Proportion of elements carrying at least one gene annotated with various COG
1291	categories
1292	
1293	Table S19: List of putative and published virulence and stress resistance genotypes in <i>Aspergillus</i>
1294	<i>fumigatus</i>
1295	
1296	Table S20: Fisher's exact test statistics for Starship enrichment by strain isolation source
1297	

1298 Table S21: Presence/absence genotyping data for the 20 high-confidence Starships in the 519  
1299 strain population using the genotyping dataset  
1300  
1301 Table S22: Metadata from RNASeq studies collected from NCBI used in the meta-analyses of  
1302 *Starship* gene expression.  
1303  
1304 Table S23: Summary of RNASeq studies collected from NCBI used in the meta-analyses of  
1305 *Starship* gene expression.  
1306  
1307 Table S24: Summary of modules assigned, and genes within them, from the WGCNA constructed  
1308 from Af293 samples.  
1309  
1310 Table S25: Significantly enriched functional terms from a series of enrichment tests (Fisher's  
1311 Exact Test) conducted on the genes within WGCNA modules.  
1312  
1313

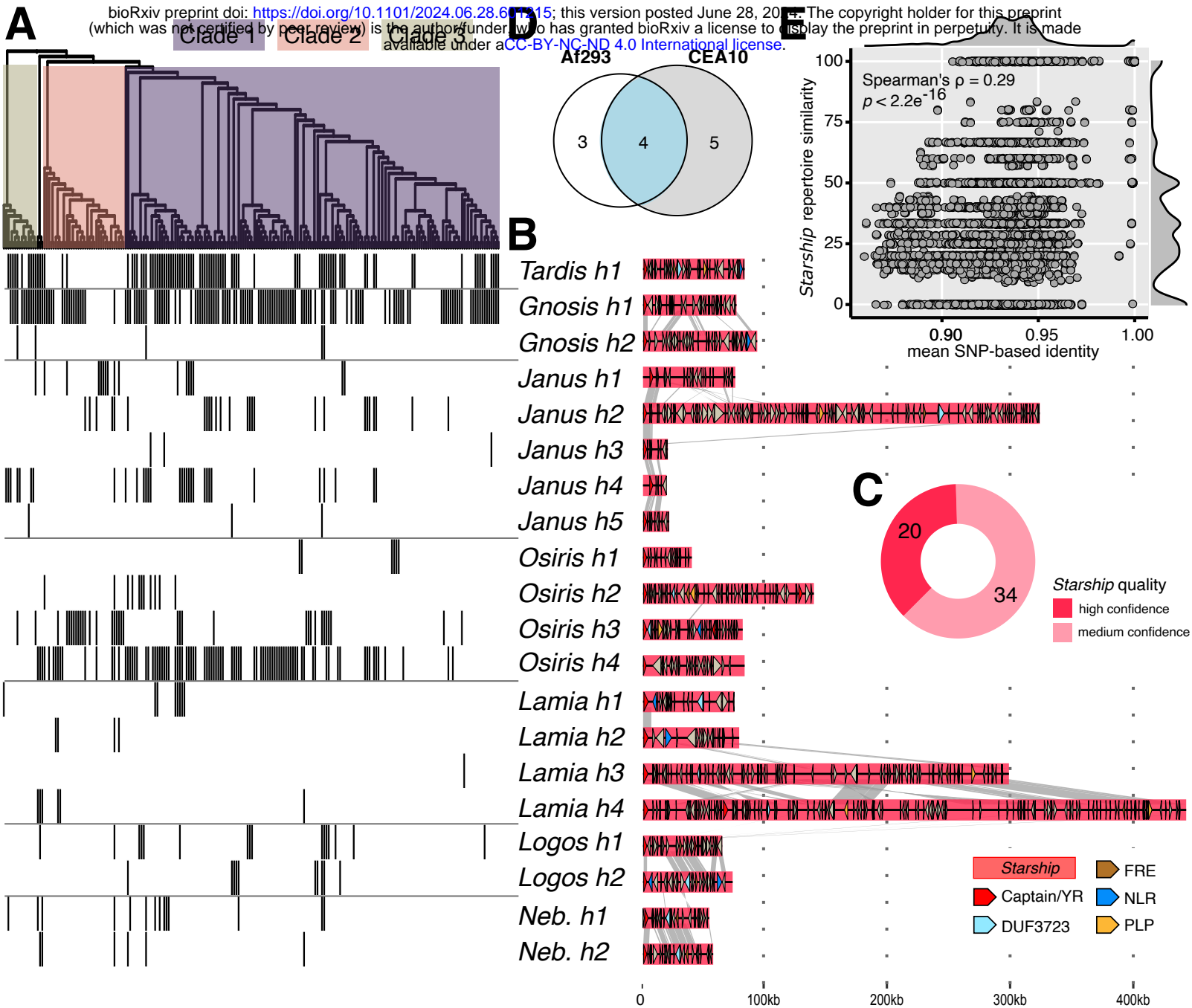


Figure 1: At least 20 distinct Starships carrying hundreds of protein-coding genes vary in their presence/absence across *Aspergillus fumigatus* strains. A) Top: a SNP-based maximum likelihood tree of 220 *A. fumigatus* strains, color-coded according to phylogenetic clade (sensu Lofgren et al., 2022)9. Bottom: A heatmap depicting the presence (gray) and absence (white) of 20 high-confidence Starships in each isolate. B) Schematics and sequence alignments of the type elements from 20 high-confidence Starships, where links between schematics represent alignable regions  $\geq 500$ bp and  $\geq 80\%$  nucleotide sequence identity and arrows represent predicted coding sequences. C) A donut chart summarizing the number of distinct types of Starships by the quality of their prediction. D) A Venn diagram indicating the number of shared and unique high-confidence Starships in the reference strains Af293 and CEA10 (Table S7). E) A scatterplot depicting pairwise comparisons of SNP-based Identity by State (IBS) and Jaccard similarity in high-confidence Starship presence/absence profiles between 150 Clade 1 strains (Table S8).

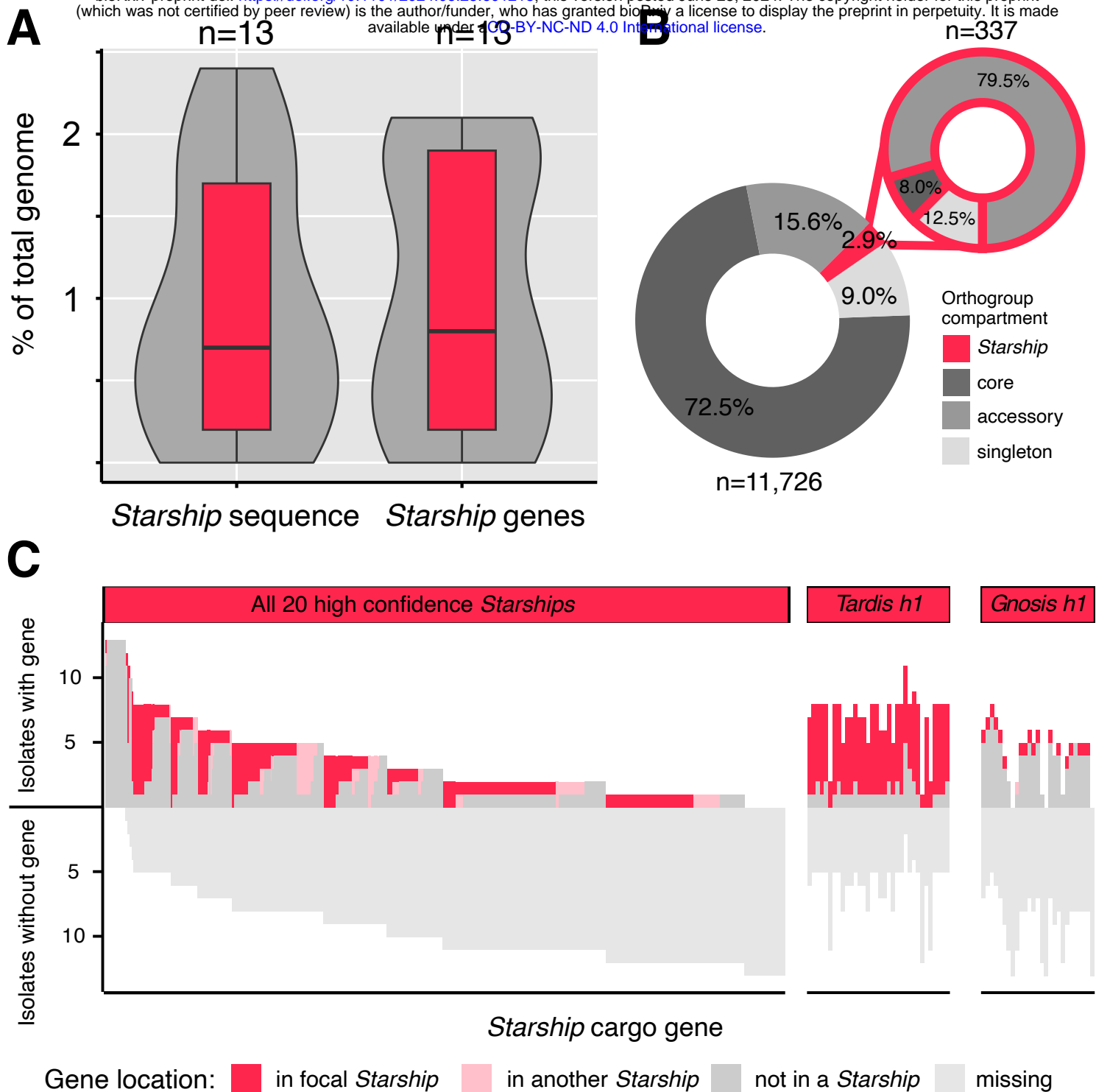


Figure 2: Starships are enriched in accessory genes whose presence/absence and genomic location vary across *Aspergillus fumigatus* strains. All panels visualize data derived from 13 reference-quality *A. fumigatus* assemblies and the 20 high-confidence Starships ( $n = 459$  elements total). A) Box-and-whisker plots summarizing the total percentage of nucleotide sequence and predicted genes carried by Starships per genome. B) Donut charts summarizing the percentages of gene orthogroups in the core, accessory, singleton, and Starship-associated compartments of the *A. fumigatus* pangenome (Table S10). C) Iceberg plots summarizing the genomic locations of the single best BLASTp hits ( $\geq 90\%$  identity,  $\geq 33\%$  query coverage) to the cargo genes from the type elements of all 20 high-confidence Starships (left) and two individual Starships (right; Table S12). Each column in the iceberg plot represents a cargo gene and is color-coded according to the genomic location of hits (full dataset in Fig. S4).

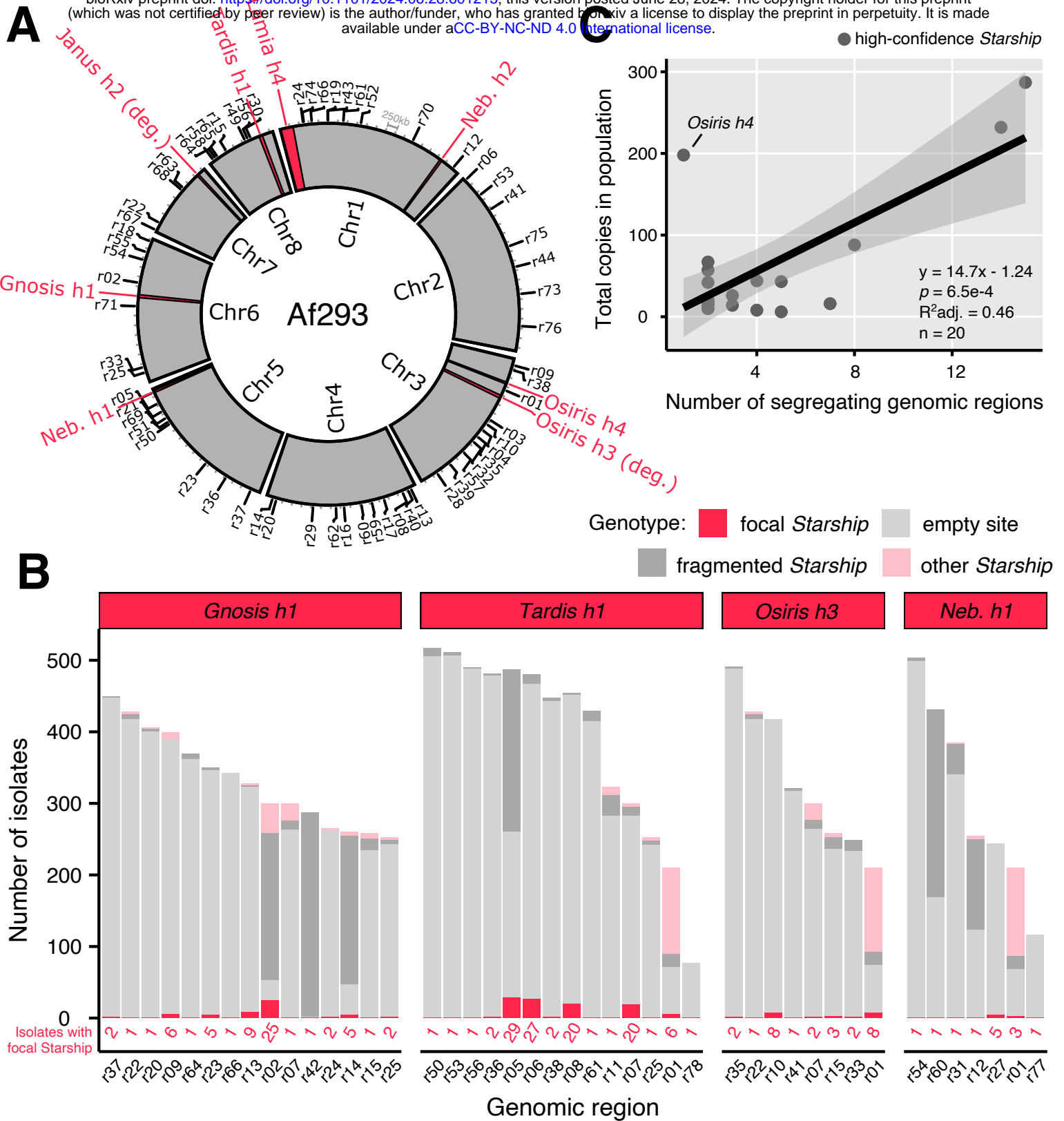


Figure 3: Starships and their insertion sites are distributed across all major chromosomes in the *Aspergillus fumigatus* genome. A) A Circos plot summarizing all inserted Starships (in red) and all genomic regions containing either an empty insertion site or a fragmented Starship (in black, along perimeter and labeled with the r prefix) in the 8 chromosomes of the *A. fumigatus* reference strain Af293 (Table S14). All genomic regions contain a Starship insertion in some other individual from the 519 strain population. B) Barcharts summarizing the genotypes of segregating genomic regions associated with the four most active high-confidence elements in the *A. fumigatus* 519 strain population (Table S16; full dataset in Fig. S6). If an isolate did not have any Starships within a given region, it was assigned either an “empty” or “fragmented” genotype (Methods). C) A scatterplot summarizing the relationship between the number of genomic regions containing a given Starship and the total number of copies of that Starship in the 519 *A. fumigatus* strain population, where each point represents one of the 20 high-confidence Starships. A line derived from a linear regression model is superimposed, with shaded 95% confidence intervals drawn in gray.

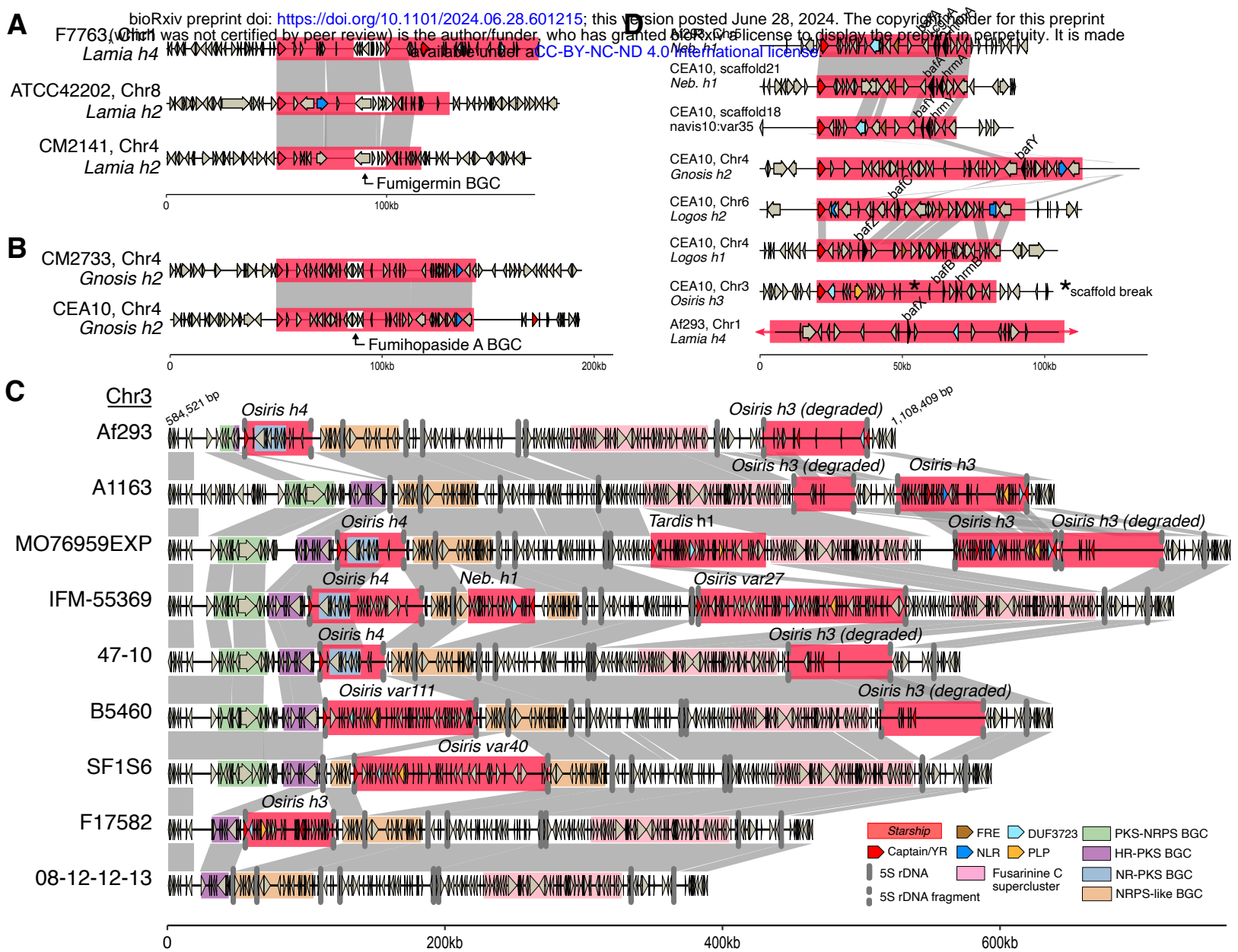


Figure 4: Starships mobilize adaptive traits and generate allelic diversity among *Aspergillus fumigatus* strains. Schematics and alignments of: A) Starship *Lamia h2* and *h4*, which carry the biosynthetic gene cluster (BGC) encoding the polyketide secondary metabolite Fumigermin39, shown inserted at 3 independent sites. B) Starship *Gnosis h2* carrying the BGC encoding the terpene secondary metabolite Fumihopaside A32, shown inserted at 2 independent sites. C) a large region on Chromosome 3 previously identified as an idiomorphic BGC30 containing multiple segregating Starship insertions and various combinations of putative BGCs, including a non-reducing polyketide synthase (NR-PKS) BGC carried by Starship *Osiris h4*. Starships from the *Osiris navis* specifically insert in 5S rDNA sequence and are predicted to fragment it (annotated by two vertical gray bars). D) Eight Starships in the reference strains *Af293* and *CEA10* that all carry homologs of biofilm architecture factor A (*bafA*)<sup>28</sup>. Starship *Nebuchadnezzar h1* (*Neb. h1*) carries *bafA* as part of the HAAC (*hrmA*-associated gene cluster), while Starship *navis10-var35* carries *bafB* as part of HBAC and Starship *Osiris h3* carries *bafC* as part of HCAC<sup>28</sup>. Only a portion of Starship *Lamia h4* is visualized for figure legibility. All data for A-D was collected from the 519 *A. fumigatus* strain population (Table S5). Links between schematics represent alignable regions  $\geq 5000$ bp and  $\geq 95\%$  nucleotide sequence identity and arrows represent predicted coding sequences. Abbreviations: polyketide synthase (PKS); non-ribosomal peptide synthetase (NRPS); highly reducing (HR).

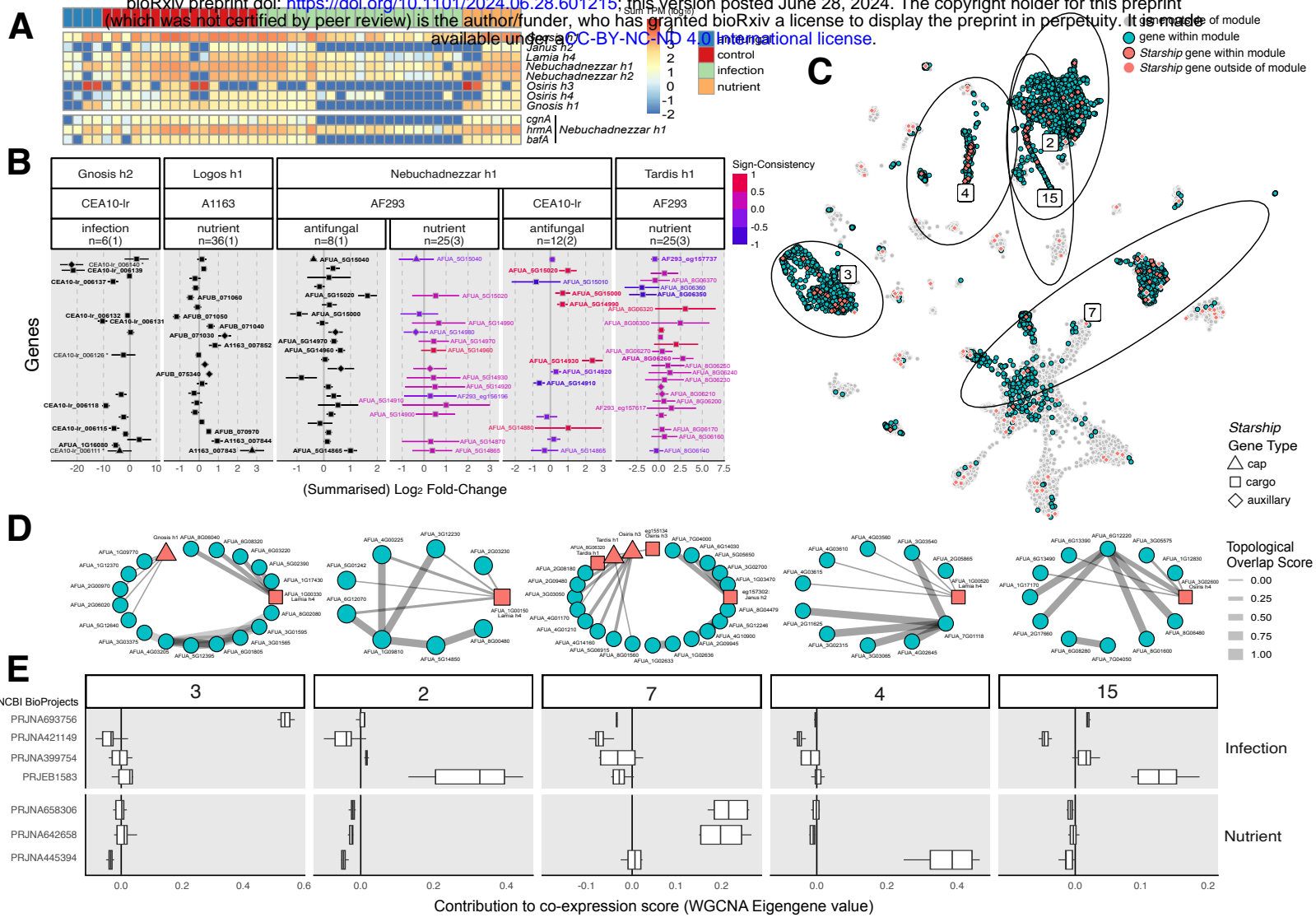


Figure 5: A) A heatmap of transcript abundances (log<sub>10</sub>TPM) of Starship captain tyrosine recombinase genes (top) and genes within the hrmA-associated cluster (HAC; bottom), collapsed across treatment replicates, for 11 RNAseq studies from *A. fumigatus* Af293. B) Results from differential expression (DE) tests for select Starships, treatment categories, and strain combinations. Only genes with valid output from DE tests are shown, and only genes with significantly DE are labeled with gene codes. Genes with extreme count outliers, as determined by Cook's Distance in DESeq2, do not have valid p-values and are labeled with an asterisk ("\*"). DE based on a single study are shown as log<sub>2</sub> fold-change (log<sub>2</sub>FC) in black with standard error bars, whereas DE genes identified across multiple studies are represented with summarized log<sub>2</sub>FC values from a random effects model (REM) and coloured by "sign-consistency", the number of studies that reported DE in the positive (+1) or negative (-1) direction, centered around 0. Labels in bold font represent DEGs that are significantly DE in more than one study. C) The results of a weighted gene co-expression network analysis (WGCNA) constructed from 14 "antifungal", "infection", and "nutrient" RNAseq studies represented using UMAP clustering based on the co-expression eigengene values for all genes in the *A. fumigatus* Af293 genome. Non-Starship genes present within modules of interest are shown in blue, while all Starship genes are shown in red, with those genes within modules of interest having a black outline. D) Genes within modules that were significantly associated with samples from specific treatment categories or studies were used to construct sub-networks which contained the top 10 edges in the network that were made between any pair of genes or any gene and a Starship captain. The connections between genes (edges) are based on the topological overlap matrix (TOM) for each module, and have been 0-1 scaled. E) Boxplots of eigengene values from WGCNA, akin to a weighted average expression profile, indicate the extent of co-expression (correlation) of the genes present within each module. Pairwise comparisons of module eigengene values determined if a module was significantly associated with samples from specific treatment categories or studies (Fig. S15).